HHS Public Access

Author manuscript

Cell Rep. Author manuscript; available in PMC 2021 December 29.

Published in final edited form as:

Cell Rep. 2021 December 14; 37(11): 110068. doi:10.1016/j.celrep.2021.110068.

Local non-pituitary growth hormone is induced with aging and facilitates epithelial damage

Vera Chesnokova[1], **Svetlana Zonis**[1], **Athanasia Apostolou**[2,3], **Hannah Q. Estrada**[4,5], **Simon Knott**[4], **Kolja Wawrowsky**[1], **Kathrin Michelsen**[5], **Anat Ben-Shlomo**[1], **Robert Barrett**[4,5], **Vera Gorbunova**[6], **Katia Karalis**[2], **Shlomo Melmed**[1,7,*]

[1]Pituitary Center, Department of Medicine, Cedars-Sinai Medical Center, Los Angeles, CA 90048, USA

[2]Emulate Inc, Boston, MA 02210, USA

[3]Graduate Program, Department of Medicine, National and Kapodistrian University of Athens, Athens 11527, Greece

[4]Department of Medicine, Board of Governors Regenerative Medicine Institute, Cedars-Sinai Medical Center, Los Angeles, CA 90048, USA

[5]Department of Medicine, F. Widjaja Foundation Inflammatory Bowel and Immunobiology Research Institute, Cedars-Sinai Medical Center, Los Angeles, CA 90048, USA

[6]Department of Biology, University of Rochester, Rochester, NY 14627, USA

[7]Lead contact

SUMMARY

Microenvironmental factors modulating age-related DNA damage are unclear. Non-pituitary growth hormone (npGH) is induced in human colon, non-transformed human colon cells, and fibroblasts, and in 3-dimensional intestinal organoids with age-associated DNA damage. Autocrine/paracrine npGH suppresses p53 and attenuates DNA damage response (DDR) by inducing TRIM29 and reducing ATM phosphorylation, leading to reduced DNA repair and DNA damage accumulation. Organoids cultured up to 4 months exhibit aging markers, p16, and SA-β-galactosidase and decreased telomere length, as well as DNA damage accumulation, with increased npGH, suppressed p53, and attenuated DDR. Suppressing GH in aged organoids increases p53 and decreases DNA damage. WT mice exhibit age-dependent colon DNA damage accumulation, while in aged mice devoid of colon GH signaling, DNA damage remains low, with

*Correspondence: melmed@csmc.edu.

AUTHOR CONTRIBUTIONS

V.C. and S.M. developed the hypothesis and designed the studies. V.C., S.Z., A.A., S.K., R.B., and H.Q.E. conducted the experiments, and K.W. acquired and analyzed the initial data. V.G., K.M., S.K., and K.K. provided the reagents. V.C., A.B.-S., A.A., S.M., V.G., K.M., S.K., and K.K. analyzed, discussed, and interpreted the data. V.C. and S.M. wrote the manuscript. All of the authors approved the submitted manuscript.

SUPPLEMENTAL INFORMATION

Supplemental information can be found online at https://doi.org/10.1016/j.celrep.2021.110068.

DECLARATION OF INTERESTS

The authors declare no competing interests.

elevated p53. As age-associated npGH induction enables a pro-proliferative microenvironment, abrogating npGH signaling could be targeted as anti-aging therapy by impeding DNA damage and age-related pathologies.

Graphical Abstract

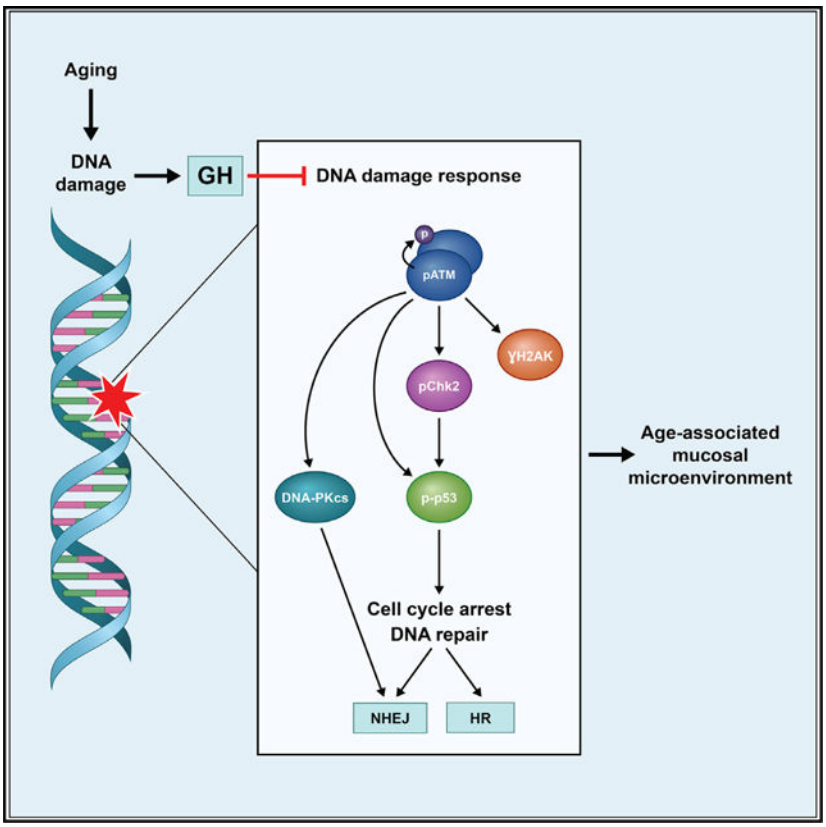

In brief

Chesnokova et al. show that non-pituitary growth hormone (npGH) is induced in aging DNA-damaged colon epithelium and suppresses DNA damage response by attenuating the phosphorylation of DNA repair proteins. npGH induction promotes DNA damage accumulation, resulting in age-associated colon microenvironment changes. Accordingly, disrupted GH signaling in aging mice prevents accumulated DNA damage.

INTRODUCTION

Biological functions decline with aging concomitantly with increased age-related disease. Age-related pathologies are driven by accumulated DNA damage and deficiencies in DNA repair that cause mutations and age-associated chromosomal aberrations. Persistent DNA damage may also block cell proliferation, resulting in senescence and apoptosis, thereby further driving the aging process (Ou and Schumacher, 2018).

DNA damage accumulates with age in wild-type (WT), non-transformed human and murine cells, as evidenced by increased phosphorylated histone 2A variant (γH2AX), a marker of double-strand DNA breaks (DSBs) (Sedelnikova et al., 2004) and unrepaired DNA damage (Dollé et al., 1997; Hasty et al., 2003; Lombard et al., 2005; Petr et al., 2020). Genomic instability resulting from defective DNA damage repair may favor cellular transformation (Negrini et al., 2010). DNA damage triggers the phosphorylation of ataxia-telangiectasia-mutated (ATM) genes, responsible for repair of single-strand DNA breaks and DSBs. ATM phosphorylates and stabilizes tumor suppressor p53, thus ensuring DNA damage repair by facilitating several DNA repair pathways. Thus, ATM plays a key role in activating both the DNA damage response (DDR) and DNA repair (Ou and Schumacher, 2018).

ATM expression and activity deteriorates with age (Feng et al., 2007; Gutierrez-Martinez et al., 2018), likely resulting in age-related functional p53 loss and leading to accumulated DNA damage and chromosomal instability (Simon et al., 2009). p53 responses to stressors such as radiation are lower in older mice (Feng et al., 2007) and in human dermal fibroblasts derived from aged individuals (Goukassian et al., 2000). Thus, the hallmarks of aging include decreased DDR activity and p53 suppression with accumulated unrepaired DNA damage, all enabling a favorable milieu for epithelial proliferation (López-Otin et al., 2013).

As pituitary growth hormone (GH) secretion declines with age, altered GH signaling has been implicated in the aging process (Ho and Hoffman, 1993) Nevertheless, a body of evidence supports the beneficial effects of GH attenuation on aging. In cell, murine, and human disease models (Brown-Borg et al., 1996; Junnila et al., 2013), the benefits of GH deficiency stem primarily from observations favoring secondary factors that extend lifespan, including enhanced insulin sensitivity, decreased hepatic protein oxidation, decreased cancer incidence, and decreased age-associated inflammation (Aguiar-Oliveira and Bartke, 2019; Bartke, 2016; Junnila et al., 2013; Spadaro et al., 2016). Offspring of Leiden study families with familial longevity and lower mortality than environmentally matched controls have lower integrated circulating GH levels (van der Spoel et al., 2016), while GH excess decreases lifespan as seen in patients with acromegaly (Chesnokova et al., 2019a; Melmed, 2020; Waters and Barclay, 2007) and in transgenic murine models overexpressing GH (Bartke, 2003). Some have suggested a negative correlation between height and longevity in humans (He et al., 2014; Samaras and Storms, 1992) and in dogs (Greer et al., 2007),

We hypothesized that adverse GH effects on aging may, at least in part, be attributed to accumulated DNA damage (Chesnokova and Melmed, 2020). In support of this premise, lymphocytes derived from acromegaly patients exhibit DNA damage with increased chromosomal aberrations (Bayram et al., 2014), while unrepaired DNA damage accumulates in the liver of a zebrafish acromegaly model (Elbialy et al., 2018). High circulating GH levels attenuate murine colon DNA repair, triggering DNA damage accumulation, while DNA damage is attenuated after blocking GH receptor (GHR) in human colon cells and in mice with abrogated GHR signaling (Chesnokova et al., 2019a).

Non-pituitary GH (npGH) synthesized locally in peripheral tissues is identical to endocrine GH1 produced by the pituitary, and acts through autocrine/paracrine mechanisms via the widely expressed GHR (Ballesteros et al., 2000) that recognizes both pituitary GH and

npGH ligands (Waters and Barclay, 2007; Waters et al., 2006). As DDR activation induces npGH (Chesnokova et al., 2013), we hypothesized that age-associated accumulated colon DNA damage induces npGH expression, which, in turn, would further constrain DNA damage repair.

Using both *in vitro* and *ex vivo* human models reflective of aging, we show here that npGH is induced and DNA damage accumulates in aged human tissues, as evidenced by increased H2AX phosphorylation (γH2AX). Furthermore, colon DNA damage is significantly increased in aged WT mice, while epithelial DNA damage remains low in age-matched $GHR^{-/-}$ mice devoid of GH signaling and in colon-specific GHR knockout mice (*GHR*colKO).

Local npGH was also induced in aged 3-dimensional (3D) intestinal organoids generated from induced human pluripotent stem cells (iPSCs) (Barrett et al., 2014; Chesnokova et al., 2019a). Organoid npGH, in turn, suppressed p53 and attenuated DNA damage repair. Effects of npGH were likely paracrine, as co-culturing GH-expressing fibroblasts with Colon Intestine-Chip microfluidic devices embedded with human colonoids led to suppressed p53/p21 and enhanced DNA damage. By contrast, suppressing GH in aged organoids prevented DNA damage.

Thus, we show that epithelial npGH is strongly induced during aging and that npGH reduces DNA repair and facilitates age-associated DNA damage accumulation. Overall, the results suggest that local colon epithelial npGH triggers a mucosal field change, creating a milieu of chromosomal instability that is favorable for neoplastic development in aging tissue.

Importantly, although there is widespread inappropriate use of GH as an “anti-aging” hormone despite the lack of compelling impact on the aging process (Blackman et al., 2002; Clemmons et al., 2014; Liu et al., 2007; Melmed, 2019), our results show that local GH signaling contributes to the tissue microenvironment, favoring development of age-related pathologies. Suppressing local npGH signaling to constrain adverse epithelial DNA damage may therefore offer a novel anti-aging therapeutic target. Results of these studies inform an innovative approach to lifespan extension (i.e., suppression rather than induction of local GH signaling).

RESULTS

Human colon DNA damage and npGH accumulate with aging

Age-associated DNA damage was assessed in non-tumorous human colon paraffin tissue samples derived from patient cohorts spanning 3 age groups: young (18–39 years), middle aged (40–60 years), and aged (61–88 years). When scored for γH2AX, 3 of 11 samples (27%) in the young cohort exhibited DNA damage, 8 of 16 (50%) exhibited DNA damage at middle age, and 8 of 18 (45%) aged samples exhibited DNA damage (Figures 1A–1C and 1J).

As we previously showed that DNA damage induces npGH (Chesnokova et al., 2013), we sought to determine whether age-dependent accumulation of DNA damage was associated

with GH expression in non-tumorous colon tissue. As npGH is expressed in neuroendocrine colon cells (Chesnokova et al., 2016), we excluded these cells from analysis.

Epithelial GH expression was detected in 16%–17% of normal colon samples derived from middle-aged and aged cohorts (38 and 42 samples, respectively) but in only 2% of the young cohort (37 samples), while the GH expression score was increased in the middle-aged cohort and further increased in the aged cohort samples ($p < 0.01$) (Figures 1D–1F and 1K). Furthermore, colon mRNA GH expression increased in both middle aged (30% of 10 samples) and aged (26% of 14 samples) versus young cohort samples (17% of 9 samples) ($p < 0.01$ and $p < 0.05$, respectively) (Figures 1G–1I). In summary, these results point to DNA damage accumulation with npGH induction in the aging colon.

DDR activation induces local npGH in murine and human colon

We next considered whether activated DDR triggers local colon npGH expression and treated mice with nutlin3 to stabilize p53 (Vassilev et al., 2004) and observed induced colon p53 and npGH (Figure 2A). In addition, in colon adenocarcinoma specimens derived from the same patients before and after DNA damaging therapies (Table S1), we observed modest pre-treatment baseline epithelial npGH expression and increased npGH expression after therapy in all 6 patient samples studied ($p < 0.01$) (Figure 2B). Enhanced GH expression was also observed in tumor-associated fibroblasts after DNA damage (Figure 2C), indicating that these findings are likely not cell specific.

DDR activates GH expression *in vitro*

We used the topoisomerase II inhibitor etoposide to produce both single-strand DNA breaks and DSBs (Walles et al., 1996) and to determine whether DDR activates GH *in vitro*. The DNA damage induced npGH in hNCC, hNCF, and HCT116 human colon adenocarcinoma cells (Figures 3A and S1A–S1C); in organoids, etoposide induced GH and GH mRNA (Figures 3B and S1D), while IGF1 and prolactin mRNA levels were unchanged (Figure S1E).

STAT5 phosphorylation, a downstream GH signal (Waters, 2016), was induced in all cell types (Figures 3A–3C and S1A–S1C). By contrast, abrogating npGH with GH small interfering RNA (siRNA) prevented etoposide from inducing pSTAT5 (Figures 3C and S1F), providing evidence that DNA damage-induced colon npGH is functionally active. Imaging of hNCC treated with etoposide for 24 h showed GH and γH2AX co-expression in multiple cells (Figure 3D).

Epithelial cells undergoing DNA damage secrete GH

To determine whether induced intracellular npGH exerts autocrine/paracrine effects, we assessed GH levels secreted into hNCC and organoid culture medium after etoposide treatment. Medium collected from hNCC at 8 and 24 h after treatment and from organoids at 4–48 h after treatment showed time-dependent GH increases after DDR activation (Figure 3E). Because hNCC and organoids express GH receptors as does human colon tissue (Chesnokova et al., 2016), these results suggest that local GH induced in response to DNA damage may subject aging tissue to autocrine/paracrine actions.

Autocrine/paracrine GH suppresses human colon cell p53

As endocrine GH suppresses murine colon p53 (Chesnokova et al., 2016), we determined whether local GH exerts similar autocrine/paracrine effects in human epithelial colon cells. Analysis of two separate hNCC lines derived from two different patients after nucleofection with hGH or infection with lentivirus expressing GH (lenti-GH) (Figures 4A, 4B and S2) as well as organoids stably expressing hGH (Figure 4C) showed suppressed p53 and concomitant GH overexpression. Cells derived from organoids infected with lenti-GH or empty vector (lenti-V) pulsed with bromodeoxyuridine (BrdU) showed p53 suppression followed by modest but significantly increased BrdU incorporation assessed by fluorescence-activated cell sorting (FACS) (Figure S3A). By contrast, GH suppression with lentivirus expressing small hairpin GH (shGH) led to decreased colony formation and colony size in hNCC (Figures S3B and S3C), indicating pro-proliferative npGH actions.

Paracrine GH effects in human Colon Intestine-Chip

To assess the paracrine effects of npGH on intestinal mucosal epithelial cells, we co-cultured hNCF infected with lenti-GH and Colon Intestine-Chip microfluidic devices (Kasendra et al., 2020) seeded with healthy colonic organoid-derived epithelial cells for 8 days. Local GH secretion from hNCF into the medium was confirmed by ELISA (338 ng/mL/1 × 10^6 cells). 5-Ethynyl-2′-deoxyuridine (EdU) (20 μM) was added on day 7, chips were fixed 24 h later and stained for EdU, and γH2AX, and EdU^+ nuclei were counted in epithelial cells. A separate set of chips seeded with epithelial cells was used to assess p53/p21 by western blot. Proliferation of chip epithelial cells increased ($p < 0.05$), likely due to decreased p53 and p21 (Figures 4D and 4E). Moreover, DNA damage accumulation was evident, with increased numbers of cells expressing γH2AX ($p < 0.01$) (Figure 4F).

Autocrine/paracrine GH suppresses DDR

Activation of ATM upon DNA damage phosphorylates H2AX, which marks damaged DNA sites to activate DDR and promote repair (Turinetto and Giachino, 2015). ATM also phosphorylates p53, further enhancing DNA repair (Blackford and Jackson, 2017). In hNCC as well as in organoids infected either with pIRES2-ZsGreen1hGH or with lenti-GH, GH overexpression suppressed the phosphorylation of ATM and DNA-protein kinase (PK)cs, both involved in DNA repair (Blackford and Jackson, 2017), and decreased phosphorylation of a target protein p53 (Figures 5A–5C).

Tip60 histone acetylase activates ATM (Jackson and Bartek, 2009) and is negatively regulated by TRIM29 (Sho et al., 2011; Sun et al., 2005). We observed that GH overexpression in hNCC and in organoids also resulted in TRIM29 induction, which in turn suppressed Tip60 (Figures 5A–5C). Similar results were observed in the second hNCC line 48 h after nucleofection with plasmid expressing GH and at 6 days after infection with lenti-GH (Figures S4A and S4B).

Autocrine/paracrine GH attenuates DNA repair

We next measured GH effects on DSB repair mechanisms, specifically error-prone non-homologous end joining (NHEJ) (Jackson and Bartek, 2009) and error-proof homologous recombination (HR) (Beucher et al., 2009; Blackford and Jackson, 2017; Chapman et

al., 2012). We nucleofected hNCC stably expressing NHEJ and HR reporter cassettes with pcDNA3.1-human GH1 (hGH1) plasmids, induced DSBs by co-transfecting with plasmid encoding I-SceI endonuclease, and measured the rejoining of DSB repair reporters. Transfection efficiency was controlled by co-transfecting with plasmid encoding DsRed (Seluanov et al., 2010). NHEJ efficiency after pcDNA3.1-hGH1 nucleofection was 0.77–0.83 and reduced at 48 h ($p < 0.05$) (Figure 5D), and HR, while low (0.05), consistent with other reports (Chitnis et al., 2014; Gatei et al., 2011), showed consistently decreased efficiency by up to 38.7% ± 3.5% ($n = 4$ independent experiments, $p < 0.05$) at 72 h.

Autocrine/paracrine GH increases unrepaired DNA damage

Examining whether npGH increases DNA damage, we observed that hNCC and organoids stably transfected with lenti-GH showed increased endogenous unrepaired DNA damage as measured by Comet assay ($p < 0.05$) (Lee and Paull, 2007) (Figures 5E and 5F). Levels of unrepaired DNA were also markedly increased in a second hNCC line in cells nucleofected with plasmid expressing GH or infected with lenti-GH (Figures S4C and S4D). Overall, these results show that npGH is induced in response to DNA damage and enhances DNA damage accumulation by interfering with both DDR and DNA repair pathways.

GH is induced in aged 3D human intestinal organoids and attenuates DDR

Following on the observed increased GH expression and DNA damage in aged human colon specimens, we “aged” organoids generated from three independent iPSC lines to recapitulate a model of aging human tissue. These organoids are composed of enterocytes, goblet cell, Paneth cells, and enteroendocrine cells and express caudal-type homeobox 2 (CDX2) (Barrett et al., 2014; Gao et al., 2009; Workman et al., 2017). Two of three iPSCs lines (lines 1 and 3) were obtained from individuals older than age 60 years old, and the third iPSC line (line 2) was derived from fibroblasts of a 30-year-old individual. Organoids generated from lines 1 and 3 were cultured for up to 2 months, at which point cell proliferation slowed significantly. By contrast, organoids generated from line 2 proliferated robustly in culture for up to 4 months. Cellular aging was confirmed in all 3 lines by increased p16, as well as by decreased telomere length ($p < 0.05$) (Figures 6A and 6B). In aged organoids, we also found increased senescence-associated β-galactosidase (SA-β-galactosidase) activity, which has been shown to increase with age (Kurz et al., 2000; Lee et al., 2006), as well as increased β-galactosidase protein expression, which correlates with SA-β-galactosidase enzymatic activity (Figures 6A and S5A).

As these *in vitro* organoid features appear to faithfully recapitulate cellular changes consistent with aging human tissue (Baker et al., 2011; Liu et al., 2019; López-Otín et al., 2013), we used this model to further study signaling mechanisms underlying human colon epithelial aging. In line 1, GH mRNA levels were induced after 1 month in culture and further increased after 2 months ($p < 0.05$) (Figure 6C), which is consistent with significantly increased npGH seen in aged organoids on both western blot and immunohistochemistry (IHC) (Figures 6D, 6E, and S5B). γH2AX was also strongly induced with prolonged culture, indicating accumulated endogenous DNA damage with *in vitro* aging. Consistent with results showing suppressed p53 in hNCC and organoids transfected with GH (Figures 4A–4C), we observed suppressed p53 at 1 and 2 months of culture,

concordant with increased npGH (Figures 6E and S5B). Similar results were obtained by culturing organoids generated from iPSC lines 2 and 3 for 4 and 2 months, respectively (Figures S6A–S6D).

Furthermore, increased npGH in aged organoids was associated with attenuated DDR, with suppressed phosphorylation of both ATM and DNA-PKcs and lower levels of phosphorylated p53 (Figures 6E and S5B). These results suggest that suppressed DDR activity leads to accumulated unrepaired DNA damage, as also evidenced by γH2AX induction (Figures 6E and S5B).

After 2 months in culture, aged organoids infected with GH shRNA showed increased p53 (Figures 6F and S7A) and decreased DNA damage measured by Comet assay ($p < 0.01$) (Figure 6G), indicating a requirement for npGH in age-related DNA damage accumulation in this model.

GH signaling deficiency attenuates *in vivo* colon DNA damage in aging mice

To confirm our results obtained in aged organoids, we studied aged WT and $GHR^{-/-}$ mice *in vivo*. Colon DNA damage was significantly increased in old (24-month-old) versus young (3-month-old) WT mice ($p < 0.01$), but, strikingly, was not increased in aged $GHR^{-/-}$ mice (Figures 7A and S7B), likely due to p53 induction. We also generated transgenic mice with colon-specific *GHR* excision (Car1-Cre/$GHR^{flox/flox}$,*GHR*colKO) (Figure S7D). Control mice were derived from the same breeding, but they did not harbor the Cre enzyme. Colon DNA damage was much reduced in 20-month-old male *GHR*colKO mice with GHR excision compared to control mice, but not in the small intestine with intact GHR (Figure 7D). Thus, it appears that DNA is repaired more efficiently in mice devoid of GH signaling, likely due to the higher colon p53 expression we observed in both $GHR^{-/-}$ and in *GHR*colKO animals (Figures 7B, 7C, 7E, S7C, and S7E). These *in vivo* results buttress our hypothesis that npGH enhances age-associated colon DNA damage accumulation.

DISCUSSION

We show here that npGH increases with age in human colon tissue and in 3D human intestinal organoids. We demonstrate several lines of evidence suggesting that in aged human colon tissue, npGH is induced by DNA damage, as observed in human models, including epithelial non-tumorous cells, normal colon fibroblasts, organoids, and colon cancer tissue of patients undergoing DNA damaging therapies; we also show similar findings *in vivo* in the colons of mice with activated DDR.

Using 3D human intestinal organoids, we observed increased p16, senescence, and telomere shortening, all consistent with age-associated changes in human tissue (Baker et al., 2011; Liu et al., 2019; López-Otín et al., 2013). Despite the limitations of the organoid model, our results support intestinal organoids as a faithful human recapitulation to study signaling mechanisms underlying age-associated colon changes (Hu et al., 2018).

We found that local npGH, acting in an autocrine/paracrine fashion, suppresses p53 and increases neighboring cell proliferation. Induced GH also suppresses DDR and DNA repair,

further enhancing DNA damage accumulation. The results are also consistent with the observed effects on DNA damage accumulation within GH-secreting human pituitary tumors (Ben-Shlomo et al., 2020).

GH actions in normal colon tissue favor the development of a pro-proliferative milieu that may underlie age-related increased rates of colon polyps, exemplified by age-associated DNA damage and chromosomal instability as the drivers of colon cancer prevalence in patients older than 50 years (Aunan et al., 2017). The age-related increased DNA damage we show here is also consistent with reports that γH2AX increases linearly with age in normal colon specimens (Risques et al., 2008). Our observed marked upregulation of γH2AX in aging organoids is indicative of DNA damage accumulation, as γH2AX marks DNA damage sites to attract DNA repair proteins (Turinetto and Giachino, 2015).

These results may be seemingly inconsistent with the fact that GH induced in aging cells suppresses H2AX phosphorylation. However, we interpret these observations to show that GH decreases DDR activity by decreasing phosphorylation of ATM, which, in turn, decreases (but does not completely abolish) the phosphorylation of downstream proteins including H2AX. When DDR is not appropriately activated, DNA repair is altered, but γH2AX still accumulates as it marks unrepaired DNA damage sites. Thus, γH2AX levels observed in aging human tissue and organoids reflect a net result of DDR activity and the amount of unrepaired DNA.

DNA damage may accumulate in aging tissue due to the loss of base excision repair, likely from the loss of p53 response to DNA damage (Cabelof et al., 2006; Simon et al., 2009, 2012). In our experiments, p53 declined in colon cells and organoids expressing npGH, consistent with earlier findings of GH suppressing p53 (Chesnokova et al., 2016). By contrast, aged *GHR*$^{-/-}$ mice, which are resistant to cancer and have a longer lifespan (Basu et al., 2018), as well as colon-specific *GHR*colKO mice exhibit an increased expression of colon p53, likely enhancing DNA repair. As GH suppresses p53 (Chesnokova et al., 2013), npGH induction may result in changes in the local microenvironment consistent with age-associated decreased p53 (Feng et al., 2007; Goukassian et al., 2000). The GH promoter contains a p53 binding site (Chesnokova et al., 2013), and DNA damage-induced p53 activates GH expression (Chesnokova et al., 2013, 2019a). Thus, our results show that in aged organoids, DNA damage accumulation induces npGH, which, in turn, down-regulates p53.

Importantly, as npGH is secreted locally from DNA-damaged cells, a paracrine action for secreted GH on neighboring cells could be operative. While co-culturing GH-expressing hNCF with the Colon Intestine-Chip, we observed increased DNA damage and proliferation and downregulated p53/p21 in chip-embedded epithelial cells exposed to the paracrine effects of fibroblast-derived npGH. These results suggest that local npGH induced with aging in human tissue alters the tissue microenvironment by suppressing tumor suppressor proteins and enhancing epithelial proliferation and DNA damage.

The results are consistent with observations that exogenous GH treatment increases proliferative capacity, colony formation, and metastases in DJ-1 KO mice (Chien et al.,

2016), and with evidence that GH induction in human tumor cells is associated with the progression of several cancers (Perry et al., 2017); these comport with our results showing fewer colony formations and smaller colony size with GH suppression.

DNA damage repair pathways protect against chromosomal instability that drives cellular transformation (Negrini et al., 2010). For example, Tip60 activates ATM (Jackson and Bartek, 2009), and ATM, a central regulator of DDR, phosphorylates and stabilizes p53. Aging cells exhibit reduced ATM and p53 suppression, as well as DNA repair dysregulation with subsequent unrepaired DNA damage (Lan et al., 2019). Thus, in colon cells, DNA damage accumulates with age (Risques et al., 2008; Schumacher et al., 2008), at least in part due to declining DDR efficiency (Jackson and Bartek, 2009), and suppressed p53 in response to γ-irradiation in aging mice was attributed to age-related decline in p53-stabilizing ATM (Feng et al., 2007). In our experiments, npGH induced in response to DNA damage also suppressed Tip60, which likely led to decreased DNA repair as evidenced by attenuated ATM and p53 phosphorylation, respectively. These results suggest that local npGH overexpression may contribute to age-related dysregulated DDR and DNA repair. In aged organoids, GH induction attenuated DDR, while GH suppression activated DDR, as evidenced by decreased DNA damage. These results are supported by our earlier observations that blocking GH signaling in hNCC led to decreased DNA damage (Chesnokova et al., 2019a). Furthermore, we show that colon DNA damage does not accumulate in colon-targeted *GHR*colKO mice with excised *GHR*, but it did accumulate in the small intestine, where *GHR* was intact. These results, along with our demonstration that aged $GHR^{-/-}$ mice do not accumulate colon DNA damage, provide *in vivo* support for the hypothesis that local npGH induction with age may render cells susceptible to transformation and perhaps also contribute to cancer therapy resistance, as has been suggested (Basu and Kopchick, 2019).

The results shown here also raise the possibility that GH effects may be mediated by insulin-like growth factor 1 (IGF1). Unlike GH, IGF1 signaling activates DNA repair in non-tumorous and tumorous cells (Chesnokova and Melmed, 2020; Chitnis et al., 2014; Turney et al., 2012), and we have shown that GH suppression of p53 and induction of DNA damage occur independent of IGF1 in normal colon tissue (Chesnokova et al., 2019a, 2019b). However, in cells and tissues in which GH activates IGF1, the latter growth factor may also signal in a cell-specific manner to counteract GH action on genome stability.

The findings suggest that npGH induced in aging colon tissue in response to accumulated DNA damage facilitates further DNA damage and appears to be an adverse determinant of DNA damage repair. Extrapolation of these findings provides a platform for several potential clinical applications. As DNA damage accumulation is a hallmark of age-related diseases, targeting GH signaling to block autocrine/paracrine npGH effects may prove useful for impeding age-related epithelial DNA damage and ultimately ameliorate progression of age-related epithelial pathologies (Milman et al., 2016) Such an approach may also benefit cancer patients undergoing DNA-damaging therapies, in whom epithelial field changes engendered by autocrine/paracrine npGH action may damage normal neighboring tissue. In this regard, disrupting GH signaling with an approved GHR antagonist (List et al., 2011; Trainer et al., 2000) may confer clinical benefits. Importantly, human GH has

been inappropriately promoted as an unapproved anti-aging and strength-enhancing therapy (Giordano et al., 2008; Holt and Ho, 2019; Medeiros and Siegel Watkins, 2018; Melmed, 2019). Given the deleterious paracrine effects of npGH that we report here, long-term inappropriate GH administration as an anti-aging elixir may elicit GHR signaling and risk the development of epithelial cell DNA damage, as well as the potential activation of occult proliferative lesions.

Limitations of the study

Several limitations of the study should be considered. Using albeit well-characterized human 3D organoids limits our ability to fully recapitulate the complexity of *in vivo* human aging and the myriad colon microenvironment factors in a human *in vitro* model. Although multiple Colon Intestine-Chips were generated, they were originally derived from a surgical specimen in a single patient. Nevertheless, despite these limitations, given the uniform results obtained from multiple available models, this study opens new approaches for understanding mechanisms underlying age-associated accumulation of DNA damage and epithelial pathologies.

STAR★METHODS

RESOURCE AVAILABILITY

Lead contact—Further information and requests for resources and reagents should be directed to and will be fulfilled by the lead contact, Shlomo Melmed (melmed@csmc.edu).

Materials availability—This study did not generate new unique reagents.

Data and code availability

- All data reported in this paper will be shared by the lead contact upon request.
- This paper does not report original code.
- Any additional information required to reanalyze the data reported in this paper is available from the lead contact upon request.

EXPERIMENTAL MODEL AND SUBJECT DETAILS

Human tissue—All experiments were approved by the Cedars-Sinai Institutional Review Board (IRB #00040182). De-identified human colon adenocarcinoma specimens obtained from the Cedars-Sinai Biobank and Translational Research Core were derived from the same 6 patients before and after undergoing radiation and/or chemotherapy. Patient characteristics are summarized in Table S1. De-identified human biopsy derived colon cells used in development of Colon Intestine-Chips (described below) were provided by Dr. Mark Donowitz, Johns Hopkins University (IRB# NA_00038329). Written informed consent was received from all participants when tissues were initially collected.

For age-related studies and RNAscope assays (described below), de-identified paraffin-embedded slides of colon tissue derived from 117 specimens were obtained from the Cedars-Sinai Biobank or purchased from iSpecimen, and colon tissue arrays were purchased

from US Biomax. Biobank and iSpecimen tissues were derived from healthy individuals with no history of colorectal malignancy and included patients with diagnoses of diverticular disease, a solitary rectal ulcer syndrome, and focal active infection. US Biomax tissue arrays were designated as “normal” by a pathologist.

Mice—All experiments were approved by the Cedars-Sinai Institutional Animal Care and Use Committee (IACUC # 0009252). Animals were maintained under 12 h day/night cycle in ventilated cages and had free access to rodent chow and water.

GHR$^{-/-}$ mice (B6N[Cg]-*Ghr*$^{tm1b[KOMP]wtsi/3J}$), in which floxed GH receptor and neomycin sequence were removed, were purchased from the Jackson laboratory. As breeding was undertaken with heterozygous males and females, WT and *GHR*$^{-/-}$ mice were obtained from the same breeding, and heterozygous breeders backcrossed with C57/Bl6 WT mice at least 6 times. Both males and females were used for this study.

Colon-specific *GHR* knockout mice (*GHR*colKO) were generated by cross-breeding C57Bl6-Tg(Car1-cre) mice with *GHR*$^{flox/flox}$ mice (B6N(Cg)Ghr$^{tm1b(KOMP)Wtsi}$/3J; UC Davis KOMP Repository). Control mice were derived from the same breeding but did not have Cre enzyme (C57Bl6-Tg(Car1-cre$^{-/-}$) × B6N(Cg)Ghr$^{tm1b(KOMP)Wtsi}$/3J). All breeders were backcrossed with FVB/NJ 3 times to enhance fertility. Only males were used for this study as females were assigned to another project.

Mice were genotyped by Transnetyx in ear-notched tissue, and mice from different litters randomly assigned for experimental groups. Sample sizes are indicated in Figures 7 and S7.

Cells—Human non-tumorous colon cells (hNCC line #1 and line #2 [lot#HC1211 and lot#0145834955002, respectively]) were obtained from de-identified normal colon sections of two individuals and validated as cytokeratin 18- and 19-expressing colon epithelial cells. Donor sex and age were not available. Cells were cultured in PriGrow III Medium supplemented with 5% FBS, and with antibiotic/antimycotic solution (Gemini Bio-Products). Cells were infected or treated before passage 4 per manufacturer instructions.

Human normal colon fibroblasts (hNCF) identified by the company with vimentin, a specific fibroblast marker, were cultured in Complete Fibroblast Growth Medium at 37°C, and used after passage 1. HCT116 cells were grown in McCoy 5A media with 10% FBS and antibiotic/antimycotic solution. All cells were cultured in a humidified atmosphere at 37°C and 5% CO2.

3D human intestinal organoids—Three iPSC lines (CS03iCTR-n1, CS688iCTR-n5 and CS83iCTR-33n1) obtained from the iPSC Core at Cedars-Sinai Medical Center were derived from fibroblasts from de-identified healthy volunteer donors. Sex of the donors was not available. CS688iCTR-n5 and CS83iCTR-33n1 lines were derived from donors aged 60 and 72 years respectively, while the CS03iCTR-n1 line was derived from a 30-year-old donor. Cell lines were fully characterized for pluripotency markers, confirmed to be karyotypically normal, and maintained in an undifferentiated state on Matrigel-coated plates in mTeSR1 media under feeder-free conditions.

METHOD DETAILS

3D human intestinal organoids

Generation of human intestinal organoids (HIOs) from iPSCs: Generation of HIOs from iPSCs required multiple steps, whereby iPSCs were directed to form definitive endoderm, hindgut structures, and ultimately HIOs. To induce definitive endoderm formation, iPSCs were cultured with a high dose of Activin A (100 ng/mL) with increasing concentrations of fetal bovine serum over time (0%, 0.2%, and 2% on Days 1, 2, and 3, respectively). Wnt3A (25 ng/mL) was added on the first day of endoderm differentiation. To induce hindgut formation, cells were cultured in Advanced DMEM/F12 with 2% fetal bovine serum and FGF4 (500 ng/mL) and CHIR99021 (3 mM). After 3–4 days, free-floating epithelial spheres and loosely attached visible epithelial tubes were harvested, suspended in Matrigel, and overlaid in intestinal medium containing 2 mM CHIR99021, noggin, and epidermal growth factor (both 100 ng/mL), and B27 (1X).

Generation of epithelial-only HIOs (eHIOs): After 12–18 days, HIOs were removed from Matrigel, washed, and incubated in TrypLE Express for 20 min to yield a single cell suspension which was passed through a 30 μm filter and stained with CD326 for 30 min at 4°C. Cells were sorted by magnetic activation and EpCAM+ cells resuspended at a density of 5×10^4 cells/mL in Matrigel and overlaid with intestinal medium containing ROCK inhibitor (10 μM), SB202190 (10 μM), and A83–01 (500 nM) to generate eHIO. eHIOs were continually resorted every two weeks.

Thirty days after differentiation, eHIOs were passaged every 7–10 days, and verified as intestinal organoids composed of enterocytes, goblet cell, Paneth cells, and enteroendocrine cells, and expressed CDX2, a specific intestinal marker. eHIOs were passed for up to 4 months in intestinal organoid medium additionally enriched with A83301 and SB202190.

Human Colon Intestine-Chips—Human biopsy-derived colonoids, derived from a de-identified male donor (age not available), and isolated by approved protocols at Johns Hopkins University Institutional Review Board (IRB #NA_00038329), were kindly provided by Dr. Mark Donowitz's research group. Colonoids embedded in Matrigel were maintained in suspension in IntestiCult Organoid Growth Medium (Human), supplemented with 100 μg/mL Primocin antibiotic solution passaged every 7 days, and cultured in a humidified environment at 37°C in 5% CO2.

Colon Intestine-Chips comprise two parallel channels separated by a porous PDMS membrane (diameter: 7 μm, spacing: 40 μm), and two lateral channels for vacuum application. Colonoids were grown on the top channel, while colonic fibroblasts were seeded in the bottom channel.

For seeding on chips, colonoids were recovered from Matrigel using Cell Recovery Solution, fragmented by incubation at 37°C for 2 min in with TrypLE then diluted with PBS1X 1:1 (vol/vol) and supplemented with 10 μM Y-27632 resuspended in IntestiCult medium supplemented with 10 μm Y-27632 and 5 μm CHIR99021 and seeded into the apical

channel of the Colon Intestine-Chip at a density of 7×10^6 cells/mL. Y-27632 (10 μM) and CHIR99021 (5 μM) were maintained for 72h.

For co-culturing, fibroblasts were seeded on the basal side of the PDMS membrane prior to seeding of epithelial cells. Fibroblast suspensions (20 μL) at a density of 5×10^6 cells/mL were introduced into the basal channel of the Colon Intestine-Chips kept inverted at 37°C in a humidified environment for up to 1h. The basal channel was immersed in the same medium as the epithelial channel. On days 3 and 4 of co-culturing, Colon Intestine-Chips were acclimated to mechanical forces and stretched first at 2% then at 10% at 0.15 Hz.

Constructs and transfections—Lentiviral particles pLV-EF1p-hGH1-IRES-eGFP-WPRE expressing human GH1 and pLV-EF1p-mCherry-hGH1-IRES-eGFP-WPRE control lentiviral particles were generated at the Regenerative Medicine Institute at Cedars-Sinai.

Human GH1 was synthesized (Genewiz) and subcloned into pIRES2-ZsGreen1, pcDNA 3.1, or mCMV vectors, and verified by DNA sequencing. Sequence:
GAATTCATGGCTACAGGCTCCCGGACGTCCCTGCTCCTGGCTTTTGGCCTGCTCTG
CCTGCCCTGGCTTCAAGAGGGCAGTGCCTTCCCAACCATTCCCTTATCCAGGCTTT
TTGACAACGCTATGCTCCGCGCCCATCGTCTGCACCAGCTGGCCTTTGACACCTAC
CAGGAGTTTGAAGAAGCCTATATCCCAAAGGAACAGAAGTATTCATTCCTGCAGA
ACCCCCAGACCTCCCTCTGTTTCTCAGAGTCTATTCCGACACCCTCCAACAGGGA
GGAAACACAACAGAAATCCAACCTAGAGCTGCTCCGCATCTCCCTGCTGCTCATC
CAGTCGTGGCTGGAGCCCGTGCAGTTCCTCAGGAGTGTCTTCGCCAACAGCCTGG
TGTACGGCGCCTCTGACAGCAACGTCTATGACCTCCTAAAGGACCTAGAGGAAGG
CATCCAAACGCTGATGGGGAGGCTGGAAGATGGCAGCCCCCGGACTGGGCAGAT
CTTCAAGCAGACCTACAGCAAGTTCGACACAAACTCACACAACGATGACGCACTA
CTCAAGAACTACGGGCTGCTCTACTGCTTCAGGAAGGACATGGACAAGGTCGAGA
CATTCCTGCGCATCGTGCAGTGCCGCTCTGTGGAGGGCAGCTGTGGCTTCTAGGG
ATCC

***In vivo* injections—**For experiments requiring nutlin3 injections, nutlin3 was dissolved in DMSO and three 2-month-old C57BL/6 male mice injected i.p. at a dose of 40 mg/kg BW in 100 μL DMSO every 2 days for a total of 6 injections. Three control animals received DMSO only.

Treatment with etoposide—Etoposide was prepared as a 50 mM DMSO stock solution. Cells and 3D human intestinal organoids were treated at the indicated doses for the indicated times. *In vitro* experiments were performed in triplicate and repeated at least three times.

Experiments with Colon Intestine-Chips

Immunofluorescence: On day 8 of culture, Colon Intestine-Chips were fixed at room temperature, for 15 × min in 4% Paraformaldehyde solution. Chips were washed in both channels with PBS1x, immersed in permeabilization solution (10% Normal Donkey Serum, 0.1% Triton X-100 in PBS1x) for 30 min followed by blocking solution (10% normal donkey serum in PBS1x) for 1h at room temperature, and incubated overnight at 4°C with primary γH2AX antibody. Subsequently, chips were stained with Alexa Fluor secondary

antibody and counterstained with 50 μg/mL DAPI for 15 min. Antibody solutions were prepared using 5% normal donkey serum in PBS1X. To assess epithelial cell proliferative capacity, chips were treated with 20 μM EdU on day 7 of culture, harvested 24h later, and EdU reactivity assessed.

Imaging and imaging quantification: Fluorescent z stack images of the Colon Intestine-Chip were acquired by inverted laser-scanning confocal microscopy (Zeiss LSM 880). Five individual fields of view were acquired across each Colon Intestine-Chip and total numbers of DAPI, EdU, and γH2AX positive cells assessed using ImageJ. For western blots, epithelial cells from 4 control and 5 experimental chips were harvested and analyzed for p53 and p21 expression (Figure 4E). For EdU incorporation, 7 control and 7 experimental chips were analyzed respectively (Figure 4D); for γH2AX expression, 4 control and 4 experimental chips were analyzed (Figure 4F). For quantification, slides were coded for blinded analyses.

Transfection of cells and organoids with lentivirus particles expressing hGH1 or GH1 shRNA, or with GH1 siRN—hNCC or hNCF were plated one day before transfections or treatments and cells infected with 50 MOI pLV-EF1p-hGH1-IRES-eGFP-WPRE lentiviral particles or with empty pLV-EF1p-mCherry-IRES-eGFP-WPRE lentivector with 8 mμ/mL polybrene. Cells were harvested 1 week after infection, sorted for GFP expression by FACSAria, and used within 2 months.

Organoids were dispersed into single cell suspension, mCMV-hGH1-RFP-HYGRO or mCMV-RFP-HYGRO vector lentiviral particles (generated at Cedars-Sinai) with 8 μg/mL polybrene and Matrigel added, and cells plated into 24-well plates and overlaid with intestinal organoid medium supplemented with ROCK inhibitor to block apoptosis. Lentiviral particles expressing human GH shRNA and control sh RNA (Scramble) lentiviral particles were received as stock solutions (1 × 106 IU/200 μM in DMEM). hNCC or organoids were infected with 50 MOI lentiviral particles and 8 μg/mL polybrene added. hNCC cells were selected with puromycin, and used after passage 4. Organoids were analyzed 1 week after infection.

hNCC were nucleofected with 30 pM of GH1 siRNA or control siRNA with Amaxa Nucleofector I (program W-01). Medium was changed 24h after nucleofection, cells treated with etoposide and harvested 24h later.

Transfection of cells with pIRES2-ZsGreen1-hGH1, pcDNA 3.1hGH1, or mCMV hGH1 vectors—hNCC were plated one day before transfections or treatments. Transient transfections were carried out using 1 μg/mL plasmid DNA and 2.5 μL/mL Lipofectamine 2000. hNCC line #2 cells were nucleofected with Amaxa Nucleofector I using Amaxa Basic Nucleofector Kit for Primary Mammalian Epithelial Cells. Control cells were transfected with plasmids devoid of hGH1. Efficiency of nucleofection was > 60%. Cells were analyzed at 48 hours or 6 days after transfection (Figures S4A and S4B).

Protein analysis—For western blot analysis, cells were lysed in RIPA buffer (MilliporeSigma) with protease inhibitors (MilliporeSigma) or isolated from TRIzol and

dissolved in 1% SDS (Molecular Research Center, Inc.). Proteins were separated by SDS-PAGE, electroblotted onto Trans-Blot Turbo Transfer Pack 0.2 μm PVDF membrane (BioRad), and incubated overnight with antibodies, followed by corresponding secondary antibodies. Hikari signal enhancer kit was used to detect low abundance protein. For information about antibodies, see Key resources table.

Immunohistochemistry (IHC) and immunocytochemistry (ICC)

IHC: For IHC analysis on paraffin-embedded human tissues, primary antibodies to GH were purchased from Lifespan Biosciences. Paraffin slides were first treated at 60°C for 1h, de-paraffinized and dehydrated. Antigen retrieval was performed in 10 mM sodium citrate, and control reactions were devoid of primary antibodies. Tissues were permeabilized with 1% Triton X-100 for 1h, followed by ImmPress Excel Staining Kit-Peroxidase. De-identified slides were reviewed by 2 individuals. Specimens from both sexes were analyzed together. For GH protein expression, 37 samples were analyzed in the young cohort, 38 in the middle-aged cohort, and 42 in the aged cohort. Between 5 and 7 fields from each slide were analyzed.

For mouse specimens, rat GH antibodies from Dr. A.F. Parlow at the National Hormone and Peptide Program were used. For fluorescent stain of both human and mouse specimens after permeabilization, sections were blocked in 10% serum of the animal in which secondary antibodies were generated (goat or donkey). Primary antibodies diluted in 10% serum were added overnight, cells washed in PBS, and secondary donkey anti-rabbit Alexa Fluor 568 antibodies (for mouse specimens) or goat anti-rabbit Alexa Fluor 488 or donkey anti-mouse Alexa Fluor 568 (both for human specimens) added.

For GH and γH2AX staining, an IHC score was assigned to each sample as intensity of staining (1, weak; 2, medium; 3, strong) multiplied by estimated percentage of positive cells. For GH IHC score, specimens with > 10% GH positive cells were assessed. For γH2AX, specimens with IHC score ≥ 50 were considered positive.

Intensity of human colon adenocarcinoma staining before and after treatments was analyzed using ImageJ software (NIH). Eight fields from each specimen were analyzed. Each image was divided into 3 primary colors (green, specific staining; red, unspecific staining; blue, DAPI nuclear staining). Only green color intensity minus background (no staining) was analyzed.

ICC: hNCC were plated on top of coverslips pre-treated with ECL Extracellular Matrix in 6-well plate. After 24h, cells were treated with 20 μM etoposide or DMSO (dilution 1:1000) as control. Twenty-four hours later, cells were fixed with 4% PFA for 20 min, permeabilized with 0.25% Triton X-100 for 30 min, blocked in 10% donkey serum for 1h, and stained with mouse anti-γH2AX and rabbit anti-GH LSBio overnight. After washing with PBS, cells were stained with a mix of donkey anti-mouse Alexa Fluor 488, donkey anti-rabbit Alexa Fluor 568, Alexa Fluor 647 phalloidin, and DAPI for 2h. After washing, coverslips were removed from plates and placed on glass slides in ProlongGold.

Organoid cells were embedded in a thin layer of Matrigel, placed into the chamber slides, and layered with organoid medium. After 10 days, organoids were fixed in 4% PFA and stained inside the chamber as described above with GH LSBio, followed by goat anti-rabbit Alexa Fluor 488, Alexa Fluor 647 phalloidin, and DAPI. After washing, ProlongGold was layered in Matrigel on top of the chamber containing organoids.

Real-time PCR—Total RNA was isolated from cells with TRIzol followed by RNAeasy mini Kit After DNase I treatment (TURBO DNA free, Ambion), cDNA was synthesized from 1 μg purified RNA by the SuperScript II First-Strand cDNA synthesis system. Quantitative PCR was performed in 20 μL reactions using SsoAdvanced SYBR Green Supermix in BioRad CFX 96 Touch Real Time PCR System. For primers, see Key resources table. PCR reactions were performed in triplicate. Experiments included template-free (water) and reverse transcriptaseminus controls to prevent contamination. Relative mRNA quantities in experimental samples were determined by CFX Maestro 1.0 software, normalized to housekeeping gene as indicated, and expressed in arbitrary units as fold-difference from control.

Telomere length—Relative Telomere Length Quantification qPCR Assay was used to assess relative telomere length. DNA was isolated from TRIzol (Molecular Research Center, Inc.), and 5 ng genomic DNA per reaction used. Reactions were conducted in triplicate. Relative telomere length in experimental samples was determined by CFX Maestro 1.0 software, normalized to the kit housekeeping gene, and expressed in arbitrary units as fold-difference from control.

Comet assay—The extent of nuclear DNA damage in individual cells was assessed by analyzing accumulated DNA breaks using OxiSelect Comet Assay kit per manufacturer instructions. Single-cell alkaline electrophoresis was used for 30 min at 1 V/cm. The level of DNA damage (intensity of the staining) was measured by ImageJ as a percent of damaged DNA in the tail of the entire cell DNA, multiplied by the length of the tail (tail DNA % × tail moment length = Olive tail moment). Values were obtained from at least 3 independent experiments.

Colon tissue was resected from *GHR*$^{-/-}$ and WT mice after sacrifice, placed in ice-cold PBS, cut lengthwise, washed twice, and placed in 5 mL ice-cold 20 mM EDTA in PBS without Mg^{2+} and Ca^{2+} in a 35 mm plastic dish. Epithelial mucosal cells were gently scraped out, minced with a scalpel, incubated for 5 min in the same EDTA solution, titrated with a 10 mL pipette, filtered through a 70 μm nylon filter, and processed as described in the manual. Animal pairs were matched by age and sex.

To evaluate DNA damage, at least 1000 nuclei per group were analyzed in colon mucosal cells *ex vivo*, and in at least 200 nuclei per group in cultured cells for each experiment.

RNAscope—*In situ* RNA hybridization was performed with RNAscope 2.5 HD Detection Reagent-RED and human GH1 probe (REF 539081) according to manufacturer protocols. Ubiquitous mRNA Mm-Ppib (REF 313911) was used as positive control, and bacterial RNA probe dabB (REF 310043) as negative control. Reagents were from Advanced Cell

Diagnostics RNAscope VS Reagent Kit-RED. Paraffin tissue sections were de-paraffinized, dehydrated, and pretreated with RNAscope Pretreatment Kit to unmask target RNA and permeabilize cells. Tissue was hybridized with target-specific double Z human GH1 probe (corresponding to bases 77–825 of human GH1; GenBank accession #NM_000515.4). For GH mRNA expression, 9 samples in the young cohort, 10 in the middle-aged cohort, and 14 in the aged cohort were analyzed. Blinded analysis was performed to quantify GH mRNA cluster signals on a cell-by-cell basis by manual counting and percent positive cells per field (× 40) calculated in 3–8 fields for each specimen. Specimens from both sexes were analyzed together.

DSB repair assays—hNCC were stably transfected with either NHEJ reporter cassette or HR reporter cassette by nucleofection with Amaxa Nucleofector-I (Lonza program #W-01) using Amaxa Basic Nucleofector Kit for Primary Mammalian Epithelial Cells. These cassettes contain the GFP gene with recognition sequences for I-SceI endonucleases for induction of DSBs. Stably transfected cells were selected for 10 days with 1 mg/mL of G418, co-transfected (by nucleofection) with 5 μg plasmid encoding I-SceI endonuclease to induce DSBs, and GH pcDNA 3.1 or pcDNA 3.1 vector and 0.5 μg plasmid encoding DsRed (pDsRed2-N1) to control for transfection efficiency. Intact reporters were negative for GFP. Upon induction of a DSB by I-SceI digestion, the functional GFP gene was reconstituted. At 48–72h after nucleofection, the number of GFP-positive cells (corresponding to efficiency of DNA DSB repair) and DsRed-positive cells (indicating efficiency of transfection) was determined by FACS, and the ratio between GFP-positive and DsRed-positive cells used as a measure of DSB repair efficiency. NHEJ repair efficiency was 0.77–0.83 in hNCC and HR efficiency was approximately 0.05 in control cells, consistent with other reports. For each nucleofection, a minimum of 50,000 cells was analyzed by FACS and final data analysis performed using FlowJo software. Experiments were repeated at least 3 times.

Cell proliferation assay—Asynchronized cells were pulsed with BrdU (BrdU Labeling and Detection Kit, diluted 1:1000) in medium with 5% FBS and cultured for 1h at 37°C. Cells were washed in PBS, trypsinized, fixed in glycine/70% ethanol fixative at pH 2.0 for 1h at −20°C, and immunostained with anti-BrdU mouse monoclonal antibody (BrdU Labeling and Detection Kit) for 30 min at 37°C, followed by donkey anti-mouse Alexa Fluor 488 secondary antibody for 1h at room temperature. Cells were then washed with PBS, resuspended in 1 mL PBS, and analyzed by FACScan.

Colony assay—hNCC stably infected with lentivirus expressing shScr or shGH were plated in a 6-well plate in PriGrowIII media supplemented with 5% FBS at concentrations of 2,000 cells/well. The experiment was conducted in duplicate. After 8 days, colonies were stained with MTT (stock in PBS 5 mg/mL, final medium concentration 0.5 mg/mL) for 1h at 37°C and 5% CO2, and assessed.

SA-β-galactosidase activity—SA-β galactosidase activity was assessed *in vitro* using a staining kit (Senescence Cells Histochemical Staining Kit). Organoids were dissociated into single cell suspension by incubating in TrypLE Express and 10,000 cells plated in intestinal organoid medium into 12-well plates pretreated with Entactin-Collagen IV-Laminin (ECL)

Cell Attachment Matrix. After 48h, cells were washed with PBS (pH 6.0), fixed, and stained with 5-bromo-4-chloro-3-indolyl-h-D-galactopyranoside (X-Gal) overnight at 37°C. Only senescent cells stain at pH 6.0.

QUANTIFICATION AND STATISTICAL ANALYSIS

Continuous data were tested across two groups with independent or paired Student's t test; for three or more groupings, ANOVA or mixed model regression (for matched data) followed by Tukey's test was used to correct for multiple group comparisons. Residuals were inspected to confirm fit of data, and where outliers were present, data were log-transformed prior to analysis. Data are presented as mean ± SEM. Differences were considered significant where two-tailed p values were < 0.05. SAS v9.4 and GraphPad v7 software were used for analysis. Data are graphed as percent of control (100%), but statistical testing was performed on raw numbers.

Supplementary Material

Refer to Web version on PubMed Central for supplementary material.

ACKNOWLEDGMENTS

Supported by NIH grants DK113998, DK007770, AG070211, and AG047200; Pfizer Award 61421295; and the Doris Factor Molecular Endocrinology Laboratory at Cedars-Sinai. The funding sources had no role in study design, data analysis, or the decision to publish. We are grateful to Shira Berman for assistance with manuscript preparation.

REFERENCES

Aguiar-Oliveira MH, and Bartke A (2019). Growth hormone deficiency: health and longevity. Endocr. Rev 40, 575–601. [PubMed: 30576428]

Aunan JR, Cho WC, and Søreide K (2017). The Biology of Aging and Cancer: A Brief Overview of Shared and Divergent Molecular Hallmarks. Aging Dis. 8, 628–642. [PubMed: 28966806]

Baker DJ, Wijshake T, Tchkonia T, LeBrasseur NK, Childs BG, van de Sluis B, Kirkland JL, and van Deursen JM (2011). Clearance of p16Ink4a-positive senescent cells delays ageing-associated disorders. Nature 479, 232–236. [PubMed: 22048312]

Ballesteros M, Leung KC, Ross RJ, Iismaa TP, and Ho KK (2000). Distribution and abundance of messenger ribonucleic acid for growth hormone receptor isoforms in human tissues. J. Clin. Endocrinol. Metab 85, 2865–2871. [PubMed: 10946895]

Barrett R, Ornelas L, Yeager N, Mandefro B, Sahabian A, Lenaeus L, Targan SR, Svendsen CN, and Sareen D (2014). Reliable generation of induced pluripotent stem cells from human lymphoblastoid cell lines. Stem Cells Transl. Med 3, 1429–1434. [PubMed: 25298370]

Bartke A (2003). Can growth hormone (GH) accelerate aging? Evidence from GH-transgenic mice. Neuroendocrinology 78, 210–216. [PubMed: 14583653]

Bartke A (2016). Healthspan and longevity can be extended by suppression of growth hormone signaling. Mamm. Genome 27, 289–299. [PubMed: 26909495]

Basu R, and Kopchick JJ (2019). The effects of growth hormone on therapy resistance in cancer. Cancer Drug Resist. 2, 827–846. [PubMed: 32382711]

Basu R, Qian Y, and Kopchick JJ (2018). Mechanisms in endocrinology: lessons from growth hormone receptor gene-disrupted mice: are there benefits of endocrine defects? Eur. J. Endocrinol 178, R155–R181. [PubMed: 29459441]

Bayram F, Bitgen N, Donmez-Altuntas H, Cakir I, Hamurcu Z, Sahin F, Simsek Y, and Baskol G (2014). Increased genome instability and oxidative DNA damage and their association with IGF-1 levels in patients with active acromegaly. Growth Horm. IGF Res 24, 29–34. [PubMed: 24382376]

Ben-Shlomo A, Deng N, Ding E, Yamamoto M, Mamelak A, Chesnokova V, Labadzhyan A, and Melmed S (2020). DNA damage and growth hormone hypersecretion in pituitary somatotroph adenomas. J. Clin. Invest 130, 5738–5755. [PubMed: 32673291]

Beucher A, Birraux J, Tchouandong L, Barton O, Shibata A, Conrad S, Goodarzi AA, Krempler A, Jeggo PA, and Löbrich M (2009). ATM and Artemis promote homologous recombination of radiation-induced DNA double-strand breaks in G2. EMBO J. 28, 3413–3427. [PubMed: 19779458]

Blackford AN, and Jackson SP (2017). ATM, ATR, and DNA-PK: The Trinity at the Heart of the DNA Damage Response. Mol. Cell 66, 801–817. [PubMed: 28622525]

Blackman MR, Sorkin JD, Münzer T, Bellantoni MF, Busby-Whitehead J, Stevens TE, Jayme J, O'Connor KG, Christmas C, Tobin JD, et al. (2002). Growth hormone and sex steroid administration in healthy aged women and men: a randomized controlled trial. JAMA 288, 2282–2292. [PubMed: 12425705]

Brown-Borg HM, Borg KE, Meliska CJ, and Bartke A (1996). Dwarf mice and the ageing process. Nature 384, 33.

Cabelof DC, Raffoul JJ, Ge Y, Van Remmen H, Matherly LH, and Heydari AR (2006). Age-related loss of the DNA repair response following exposure to oxidative stress. J. Gerontol. A Biol. Sci. Med. Sci 61, 427–434. [PubMed: 16720738]

Chapman JR, Taylor MR, and Boulton SJ (2012). Playing the end game: DNA double-strand break repair pathway choice. Mol. Cell 47, 497–510. [PubMed: 22920291]

Chesnokova V, and Melmed S (2020). Peptide hormone regulation of DNA damage responses. Endocr. Rev 41, 519–537.

Chesnokova V, Zhou C, Ben-Shlomo A, Zonis S, Tani Y, Ren SG, and Melmed S (2013). Growth hormone is a cellular senescence target in pituitary and nonpituitary cells. Proc. Natl. Acad. Sci. USA 110, E3331–E3339. [PubMed: 23940366]

Chesnokova V, Zonis S, Zhou C, Recouvreux MV, Ben-Shlomo A, Araki T, Barrett R, Workman M, Wawrowsky K, Ljubimov VA, et al. (2016). Growth hormone is permissive for neoplastic colon growth. Proc. Natl. Acad. Sci. USA 113, E3250–E3259. [PubMed: 27226307]

Chesnokova V, Zonis S, Barrett R, Kameda H, Wawrowsky K, Ben-Shlomo A, Yamamoto M, Gleeson J, Bresee C, Gorbunova V, and Melmed S (2019a). Excess growth hormone suppresses DNA damage repair in epithelial cells. JCI Insight 4, e125762.

Chesnokova V, Zonis S, Barrett RJ, Gleeson JP, and Melmed S (2019b). Growth Hormone Induces Colon DNA Damage Independent of IGF-1. Endocrinology 160, 1439–1447. [PubMed: 31002310]

Chien CH, Lee MJ, Liou HC, Liou HH, and Fu WM (2016). Growth hormone is increased in the lungs and enhances experimental lung metastasis of melanoma in DJ-1 KO mice. BMC Cancer 16, 871. [PubMed: 27825319]

Chitnis MM, Lodhia KA, Aleksic T, Gao S, Protheroe AS, and Macaulay VM (2014). IGF-1R inhibition enhances radiosensitivity and delays double-strand break repair by both non-homologous end-joining and homologous recombination. Oncogene 33, 5262–5273. [PubMed: 24186206]

Clemmons DR, Molitch M, Hoffman AR, Klibanski A, Strasburger CJ, Kleinberg DL, Ho K, Webb SM, Bronstein MD, Bouillon R, et al. (2014). Growth hormone should be used only for approved indications. J. Clin. Endocrinol. Metab 99, 409–411. [PubMed: 24423315]

Dollé ME, Giese H, Hopkins CL, Martus HJ, Hausdorff JM, and Vijg J (1997). Rapid accumulation of genome rearrangements in liver but not in brain of old mice. Nat. Genet 17, 431–434. [PubMed: 9398844]

Elbialy A, Asakawa S, Watabe S, and Kinoshita S (2018). A zebrafish acromegaly model elevates DNA damage and impairs DNA repair pathways. Biology (Basel) 7, E47. [PubMed: 30336646]

Feng Z, Hu W, Teresky AK, Hernando E, Cordon-Cardo C, and Levine AJ (2007). Declining p53 function in the aging process: a possible mechanism for the increased tumor incidence in older populations. Proc. Natl. Acad. Sci. USA 104, 16633–16638. [PubMed: 17921246]

Gao N, White P, and Kaestner KH (2009). Establishment of intestinal identity and epithelial-mesenchymal signaling by Cdx2. Dev. Cell 16, 588–599. [PubMed: 19386267]

Gatei M, Jakob B, Chen P, Kijas AW, Becherel OJ, Gueven N, Birrell G, Lee JH, Paull TT, Lerenthal Y, et al. (2011). ATM protein-dependent phosphorylation of Rad50 protein regulates DNA repair and cell cycle control. J. Biol. Chem 286, 31542–31556. [PubMed: 21757780]

Giordano R, Bonelli L, Marinazzo E, Ghigo E, and Arvat E (2008). Growth hormone treatment in human ageing: benefits and risks. Hormones (Athens) 7, 133–139. [PubMed: 18477550]

Goukassian D, Gad F, Yaar M, Eller MS, Nehal US, and Gilchrest BA (2000). Mechanisms and implications of the age-associated decrease in DNA repair capacity. FASEB J. 14, 1325–1334. [PubMed: 10877825]

Greer KA, Canterberry SC, and Murphy KE (2007). Statistical analysis regarding the effects of height and weight on life span of the domestic dog. Res. Vet. Sci 82, 208–214. [PubMed: 16919689]

Gutierrez-Martinez P, Hogdal L, Nagai M, Kruta M, Singh R, Sarosiek K, Nussenzweig A, Beerman I, Letai A, and Rossi DJ (2018). Diminished apoptotic priming and ATM signalling confer a survival advantage onto aged haematopoietic stem cells in response to DNA damage. Nat. Cell Biol 20, 413–421. [PubMed: 29531308]

Hasty P, Campisi J, Hoeijmakers J, van Steeg H, and Vijg J (2003). Aging and genome maintenance: lessons from the mouse? Science 299, 1355–1359. [PubMed: 12610296]

He Q, Morris BJ, Grove JS, Petrovitch H, Ross W, Masaki KH, Rodriguez B, Chen R, Donlon TA, Willcox DC, and Willcox BJ (2014). Shorter men live longer: association of height with longevity and FOXO3 genotype in American men of Japanese ancestry. PLoS ONE 9, e94385. [PubMed: 24804734]

Ho KK, and Hoffman DM (1993). Aging and growth hormone. Horm. Res 40, 80–86. [PubMed: 8300054]

Holt RIG, and Ho KKY (2019). The Use and Abuse of Growth Hormone in Sports. Endocr. Rev 40, 1163–1185. [PubMed: 31180479]

Hu JL, Todhunter ME, LaBarge MA, and Gartner ZJ (2018). Opportunities for organoids as new models of aging. J. Cell Biol 217, 39–50. [PubMed: 29263081]

Jackson SP, and Bartek J (2009). The DNA-damage response in human biology and disease. Nature 461, 1071–1078. [PubMed: 19847258]

Junnila RK, List EO, Berryman DE, Murrey JW, and Kopchick JJ (2013). The GH/IGF-1 axis in ageing and longevity. Nat. Rev. Endocrinol 9, 366–376. [PubMed: 23591370]

Kasendra M, Luc R, Yin J, Manatakis DV, Kulkarni G, Lucchesi C, Sliz J, Apostolou A, Sunuwar L, Obrigewitch J, et al. (2020). Duodenum Intestine-Chip for preclinical drug assessment in a human relevant model. eLife 9, e50135. [PubMed: 31933478]

Kurz DJ, Decary S, Hong Y, and Erusalimsky JD (2000). Senescence-associated (beta)-galactosidase reflects an increase in lysosomal mass during replicative ageing of human endothelial cells. J. Cell Sci 113, 3613–3622. [PubMed: 11017877]

Lan YY, Heather JM, Eisenhaure T, Garris CS, Lieb D, Raychowdhury R, and Hacohen N (2019). Extranuclear DNA accumulates in aged cells and contributes to senescence and inflammation. Aging Cell 18, e12901. [PubMed: 30706626]

Lee JH, and Paull TT (2007). Activation and regulation of ATM kinase activity in response to DNA double-strand breaks. Oncogene 26, 7741–7748. [PubMed: 18066086]

Lee BY, Han JA, Im JS, Morrone A, Johung K, Goodwin EC, Kleijer WJ, DiMaio D, and Hwang ES (2006). Senescence-associated beta-galactosidase is lysosomal beta-galactosidase. Aging Cell 5, 187–195. [PubMed: 16626397]

List EO, Sackmann-Sala L, Berryman DE, Funk K, Kelder B, Gosney ES, Okada S, Ding J, Cruz-Topete D, and Kopchick JJ (2011). Endocrine parameters and phenotypes of the growth hormone receptor gene disrupted (GHR−/−) mouse. Endocr. Rev 32, 356–386. [PubMed: 21123740]

Liu H, Bravata DM, Olkin I, Nayak S, Roberts B, Garber AM, and Hoffman AR (2007). Systematic review: the safety and efficacy of growth hormone in the healthy elderly. Ann. Intern. Med 146, 104–115. [PubMed: 17227934]

Liu JY, Souroullas GP, Diekman BO, Krishnamurthy J, Hall BM, Sorrentino JA, Parker JS, Sessions GA, Gudkov AV, and Sharpless NE (2019). Cells exhibiting strong *p16 INK4a* promoter activation

in vivo display features of senescence. Proc. Natl. Acad. Sci. USA 116, 2603–2611. [PubMed: 30683717]

Lombard DB, Chua KF, Mostoslavsky R, Franco S, Gostissa M, and Alt FW (2005). DNA repair, genome stability, and aging. Cell 120, 497–512. [PubMed: 15734682]

López-Otín C, Blasco MA, Partridge L, Serrano M, and Kroemer G (2013). The hallmarks of aging. Cell 153, 1194–1217. [PubMed: 23746838]

Medeiros A, and Siegel Watkins E (2018). Live Longer Better: The Historical Roots of Human Growth Hormone as Anti-Aging Medicine. J. Hist. Med. Allied Sci 73, 333–359. [PubMed: 29529228]

Melmed S (2019). Pathogenesis and Diagnosis of Growth Hormone Deficiency in Adults. N. Engl. J. Med 380, 2551–2562. [PubMed: 31242363]

Melmed S (2020). Pituitary-Tumor Endocrinopathies. N. Engl. J. Med 382, 937–950. [PubMed: 32130815]

Milman S, Huffman DM, and Barzilai N (2016). The Somatotropic Axis in Human Aging: Framework for the Current State of Knowledge. Cell Metab. 23, 980–989. [PubMed: 27304500]

Negrini S, Gorgoulis VG, and Halazonetis TD (2010). Genomic instability–an evolving hallmark of cancer. Nat. Rev. Mol. Cell Biol 11, 220–228. [PubMed: 20177397]

Ou HL, and Schumacher B (2018). DNA damage responses and p53 in the aging process. Blood 131, 488–495. [PubMed: 29141944]

Perry JK, Wu ZS, Mertani HC, Zhu T, and Lobie PE (2017). Tumour-Derived Human Growth Hormone As a Therapeutic Target in Oncology. Trends Endocrinol. Metab 28, 587–596. [PubMed: 28622965]

Petr MA, Tulika T, Carmona-Marin LM, and Scheibye-Knudsen M (2020). Protecting the aging genome. Trends Cell Biol. 30, 117–132. [PubMed: 31917080]

Risques RA, Lai LA, Brentnall TA, Li L, Feng Z, Gallaher J, Mandelson MT, Potter JD, Bronner MP, and Rabinovitch PS (2008). Ulcerative colitis is a disease of accelerated colon aging: evidence from telomere attrition and DNA damage. Gastroenterology 135, 410–418. [PubMed: 18519043]

Samaras TT, and Storms LH (1992). Impact of height and weight on life span. Bull. World Health Organ 70, 259–267. [PubMed: 1600586]

Schumacher B, Garinis GA, and Hoeijmakers JH (2008). Age to survive: DNA damage and aging. Trends Genet. 24, 77–85. [PubMed: 18192065]

Sedelnikova OA, Horikawa I, Zimonjic DB, Popescu NC, Bonner WM, and Barrett JC (2004). Senescing human cells and ageing mice accumulate DNA lesions with unrepairable double-strand breaks. Nat. Cell Biol 6, 168–170. [PubMed: 14755273]

Seluanov A, Mao Z, and Gorbunova V (2010). Analysis of DNA double-strand break (DSB) repair in mammalian cells. J. Vis. Exp 43, 2002.

Sho T, Tsukiyama T, Sato T, Kondo T, Cheng J, Saku T, Asaka M, and Hatakeyama S (2011). TRIM29 negatively regulates p53 via inhibition of Tip60. Biochim. Biophys. Acta 1813, 1245–1253. [PubMed: 21463657]

Simon K, Mukundan A, Dewundara S, Van Remmen H, Dombkowski AA, and Cabelof DC (2009). Transcriptional profiling of the age-related response to genotoxic stress points to differential DNA damage response with age. Mech. Ageing Dev 130, 637–647. [PubMed: 19679149]

Simon KW, Ma H, Dombkowski AA, and Cabelof DC (2012). Aging alters folate homeostasis and DNA damage response in colon. Mech. Ageing Dev 133, 75–82. [PubMed: 22306610]

Spadaro O, Goldberg EL, Camell CD, Youm YH, Kopchick JJ, Nguyen KY, Bartke A, Sun LY, and Dixit VD (2016). Growth hormone receptor deficiency protects against age-related NLRP3 inflammasome activation and immune senescence. Cell Rep. 14, 1571–1580. [PubMed: 26876170]

Sun Y, Jiang X, Chen S, Fernandes N, and Price BD (2005). A role for the Tip60 histone acetyltransferase in the acetylation and activation of ATM. Proc. Natl. Acad. Sci. USA 102, 13182–13187. [PubMed: 16141325]

Trainer PJ, Drake WM, Katznelson L, Freda PU, Herman-Bonert V, van der Lely AJ, Dimaraki EV, Stewart PM, Friend KE, Vance ML, et al. (2000). Treatment of acromegaly with the growth hormone-receptor antagonist pegvisomant. N. Engl. J. Med 342, 1171–1177. [PubMed: 10770982]

Turinetto V, and Giachino C (2015). Histone variants as emerging regulators of embryonic stem cell identity. Epigenetics 10, 563–573. [PubMed: 26114724]

Turney BW, Kerr M, Chitnis MM, Lodhia K, Wang Y, Riedemann J, Rochester M, Protheroe AS, Brewster SF, and Macaulay VM (2012). Depletion of the type 1 IGF receptor delays repair of radiation-induced DNA double strand breaks. Radiother. Oncol 103, 402–409. [PubMed: 22551565]

van der Spoel E, Jansen SW, Akintola AA, Ballieux BE, Cobbaert CM, Slagboom PE, Blauw GJ, Westendorp RGJ, Pijl H, Roelfsema F, and van Heemst D (2016). Growth hormone secretion is diminished and tightly controlled in humans enriched for familial longevity. Aging Cell 15, 1126–1131. [PubMed: 27605408]

Vassilev LT, Vu BT, Graves B, Carvajal D, Podlaski F, Filipovic Z, Kong N, Kammlott U, Lukacs C, Klein C, et al. (2004). In vivo activation of the p53 pathway by small-molecule antagonists of MDM2. Science 303, 844–848. [PubMed: 14704432]

Walles SA, Zhou R, and Liliemark E (1996). DNA damage induced by etoposide; a comparison of two different methods for determination of strand breaks in DNA. Cancer Lett. 105, 153–159. [PubMed: 8697438]

Waters MJ (2016). The growth hormone receptor. Growth Horm. IGF Res 28, 6–10. [PubMed: 26059750]

Waters MJ, and Barclay JL (2007). Does growth hormone drive breast and other cancers? Endocrinology 148, 4533–4535. [PubMed: 17876033]

Waters MJ, Hoang HN, Fairlie DP, Pelekanos RA, and Brown RJ (2006). New insights into growth hormone action. J. Mol. Endocrinol 36, 1–7. [PubMed: 16461922]

Workman MJ, Gleeson JP, Troisi EJ, Estrada HQ, Kerns SJ, Hinojosa CD, Hamilton GA, Targan SR, Svendsen CN, and Barrett RJ (2017). Enhanced utilization of induced pluripotent stem cell-derived human intestinal organoids using microengineered chips. Cell. Mol. Gastroenterol. Hepatol 5, 669–677.e2. [PubMed: 29930984]

Highlights

- Non-pituitary growth hormone (npGH) is induced in aging DNA-damaged colon epithelium
- npGH suppresses DNA damage response and phosphorylation of DNA repair proteins
- npGH promotes DNA damage accumulation and age-associated microenvironment changes
- Aging mice devoid of GH signaling do not accumulate DNA damage

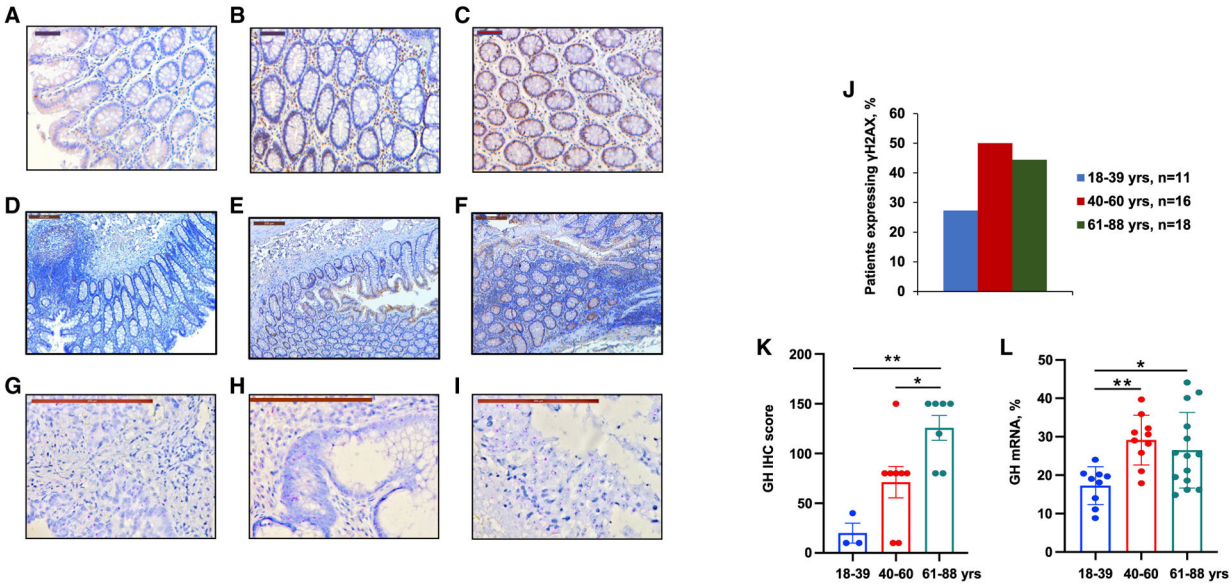

Figure 1. Human colon DNA damage and npGH increase with age

(A–C) Representative immunohistochemistry images of γH2AX expression (brown) in human colon specimens derived from (A) 27-year-old, (B) 44-year-old, and (C) 65-year-old patients. Scale bar, 200 μm.

(D–F) Representative immunohistochemistry images of GH expression (brown) in human colon specimens derived from (D) 29-year-old, (E) 42-year-old, and (F) 58-year-old patients. Scale bar, 200 μm.

(G–I) Representative images of GH mRNA expression in human colon specimens derived from (G) 23-year-old, (H) 53-year-old, and (I) 62-year-old patients. One red dot represents a cluster of GH mRNA molecules. Scale bar, 200 μm.

(J) Graph depicts percent of patients expressing γH2AX with IHC score ≥ 50. Between 5 and 7 fields were analyzed per sample.

(K) Graph depicts npGH IHC score. Between 5 and 7 fields were analyzed per sample. Only specimens with >10% GH^+ cells were assessed.

(L) Graph depicts percentage of GH $mRNA^+$ cells per field. Between 3 and 8 fields were analyzed in each slide.

In (K) and (L), each dot represents 1 patient. Results were analyzed by ANOVA followed by Tukey's test to correct for multiple groups. *$p < 0.05$, **$p < 0.01$.

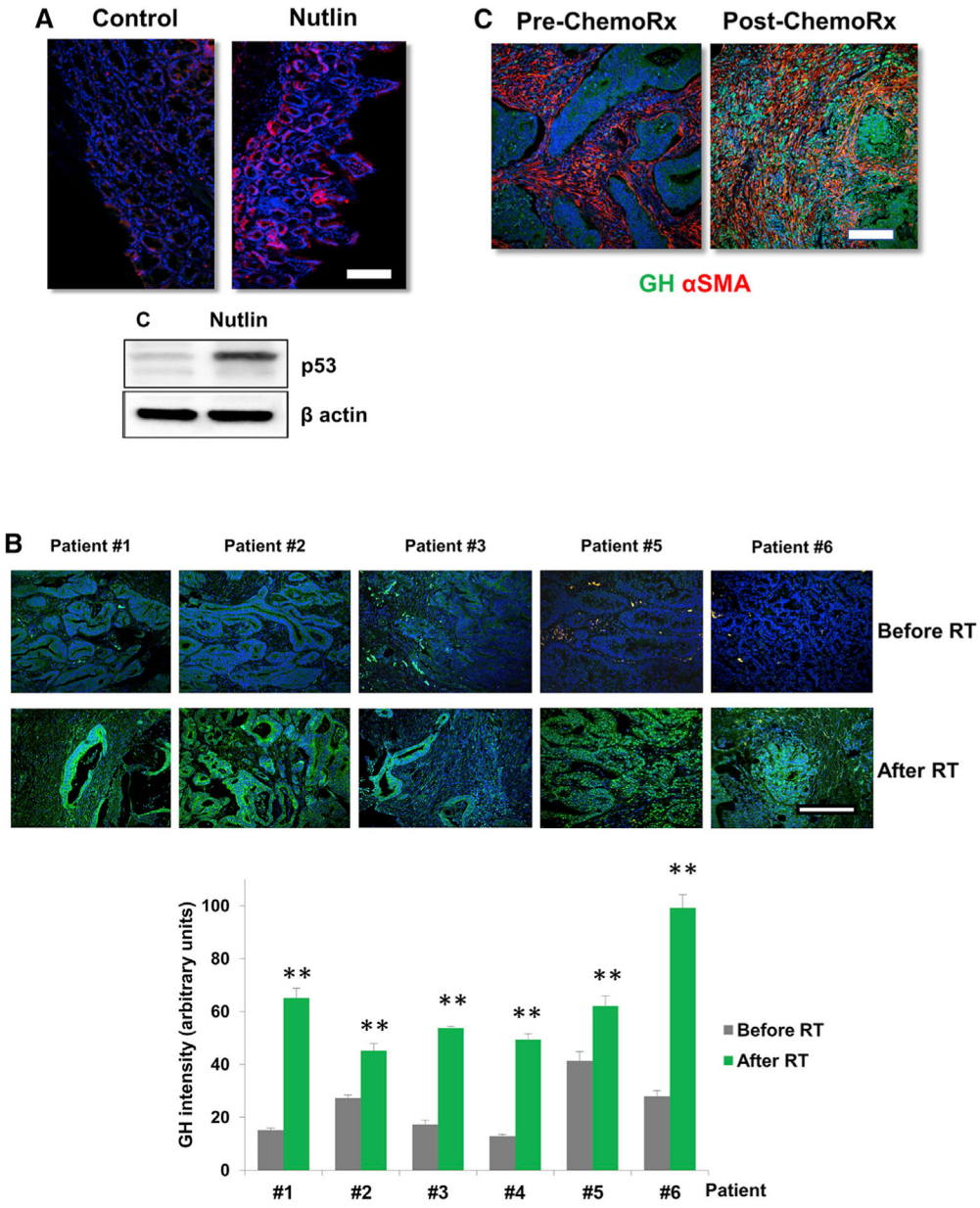

Figure 2. Murine and human colon GH is induced in response to DNA damage

(A) Upper panel, representative confocal images of colon tissue of a mouse treated with 40 mg/kg BW nutlin3 (Nutlin) or DMSO (Control) i.p. every 2 days in 6 doses (GH, red; DAPI nuclear staining, blue). Lower panel, western blot of p53 in colon tissue.

(B) Upper panel, representative human colon adenocarcinoma specimens derived from the same patients before (before RT) and after radiotherapy (after RT) (GH, green; DAPI, blue). Lower panel, intensity of GH staining in human specimens before and after RT treatment. Intensity was assessed using ImageJ, 8 fields/specimen analyzed. Results are presented as means ± SEMs and analyzed with 2-tailed t test. $^{**}p < 0.01$.

(C) Stromal tissue of human colon adenocarcinoma specimens before (pre-ChemoRx) and after chemotherapy (post-ChemoRx) (α-SMA [a marker of colon tumor-associated fibroblasts], red; GH, green; DAPI, blue). Scale bar, 100 μm.

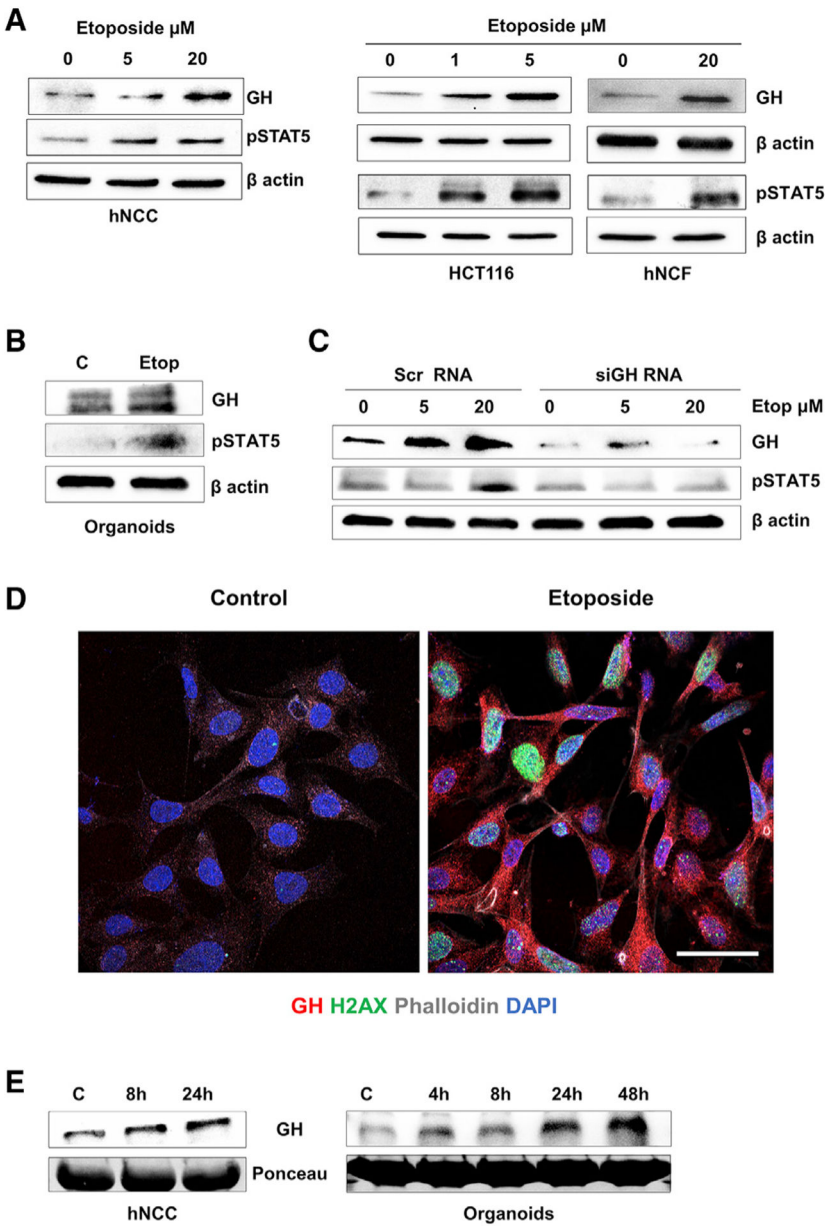

Figure 3. Activation of DNA damage pathway triggers GH expression

(A and B) Western blot of (A) hNCC, hNCF, and HCT116 cells and (B) organoids. Cells were treated with indicated doses of etoposide and analyzed 24 h later. Organoids were treated with 3 μM etoposide (Etop).

(C) hNCC nucleofected with GH siRNA (siGH RNA) or scramble RNA (Scr RNA) as control for 24 h was treated with indicated doses of etoposide (Etop) and analyzed 24 h later. ImageJ quantification of western blots is depicted in Figure S1.

(D) Representative image of hNCC treated with 20 μM etoposide for 24 h. GH, red; γH2AX, green; phalloidin, gray; DAPI, blue. Bright green nucleus indicates apoptosis. Scale bar, 20 μm. Control, untreated cells.

(E) Western blot of GH in culture medium of hNCC and organoids treated with 20 or 5 μM etoposide, respectively. Medium was collected from hNCC at 8 and 24 h and from organoids at 4–48 h after treatment. Ponceau was used as a loading control. Representative blots from at least 3 independent experiments are shown.

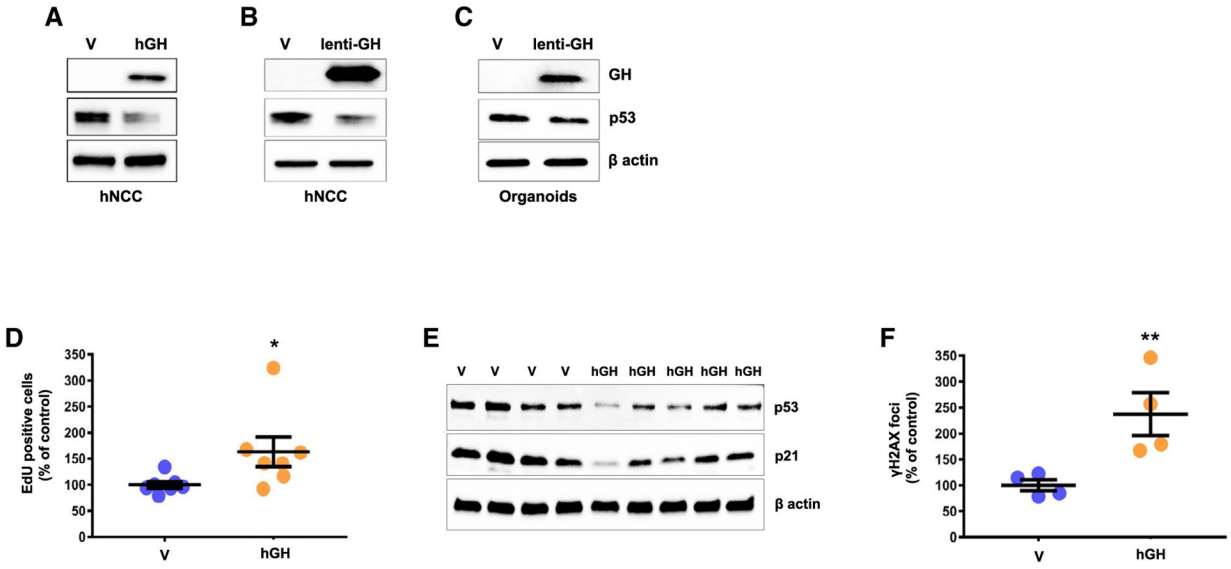

Figure 4. GH overexpression suppresses p53 and induces epithelial cell proliferation

(A–C) Western blot of p53 in (A) hNCC transfected with pIRES2-ZsGreen1hGH (hGH) or pIRES2-ZsGreen (V) and analyzed 24 h later, and (B) hNCC and (C) organoids infected with lentivirus expressing GH (lenti GH) or empty vector (V) and analyzed 6 days later. Representative blotsfrom at least 3 independent experimentsare shown.

(D–F) Paracrine GH induces epithelial cell proliferation and suppresses p53/p21. Colon Intestine-Chip multifluidic devices were co-cultured with hNCF expressing lenti-vector (V) or lenti-GH (hGH) for 8 days.

(D) Percentage of proliferating epithelial cells.

(E) Western blot of p53 and p21 in epithelial cells derived from individual chips.

(F) Percentage of $\gamma H2AX^{+}$ cells.

In (D) and (F), results are presented as means ± SEMs and analyzed with the Mann-Whitney test. Mixed-model regression was used to adjust for random effects across experimental replicates. Each dot represents an individual chip. *$p < 0.05$, **$p < 0.01$.

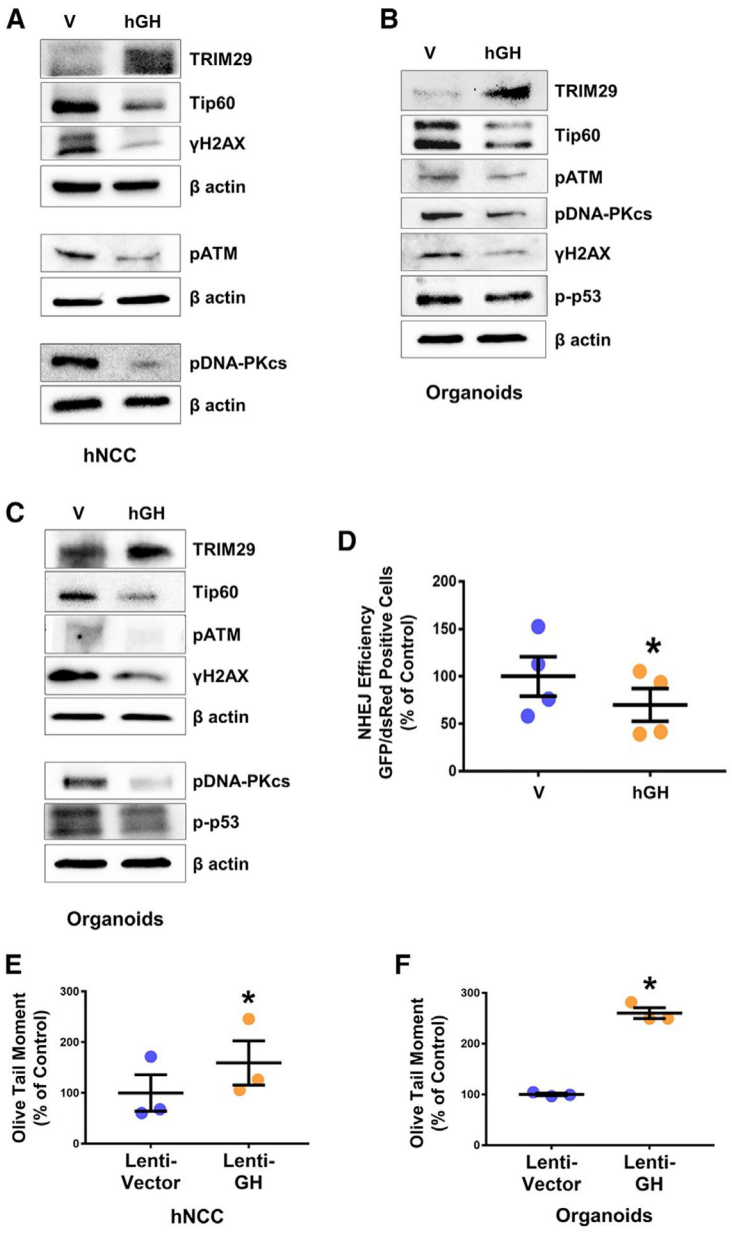

Figure 5. GH suppresses DDR, attenuates endogenous DNA repair, and enhances DNA damage accumulation

(A–C) Western blot analysis of DDR in (A) hNCC transfected with pIRES2-ZsGreen1hGH (hGH) or pIRES2-ZsGreen (V), and in organoids infected with lenti-GH (hGH) or lenti-V (V) for (B) 6 or (C) 30 days. Representative blots from at least 3 independent experiments are shown.

(D) DNA damage repair by NHEJ. pcDNA3.1 GH (hGH) or pcDNA3.1 (control, V) plasmid were co-transfected with I-SceI and DsRed into hNCC with chromosomally integrated NHEJ reporter cassette. Intact reporters were negative for GFP. Upon induction of a DSB by I-SceI digestion, the functional GFP gene was reconstituted. Cells were analyzed by FACS on day 3 after nucleofection. Mixed-model regression was used to adjust for random effects across experimental replicates. Graph shows NHEJ efficiency (% GFP^+ cells/% $DsRed^+$

cells) as percentage of controls ± SEMs in 4 independent assays. Results were analyzed with the Mann-Whitney test; *p < 0.05. Results are graphed as percentage of control, but statistical testing was performed on raw numbers. Each dot represents one experiment.
(E and F) Comet assay in (E) hNCC and (F) organoids stably infected with lenti-GH or lenti-V (control). Results shown are means ± SEMs. Each dot represents 1 experiment. Mixed-model regression was used to adjust for random effects across experimental replicates. *p < 0.05. Results are graphed as percentage of control, but statistical testing was performed on raw numbers.

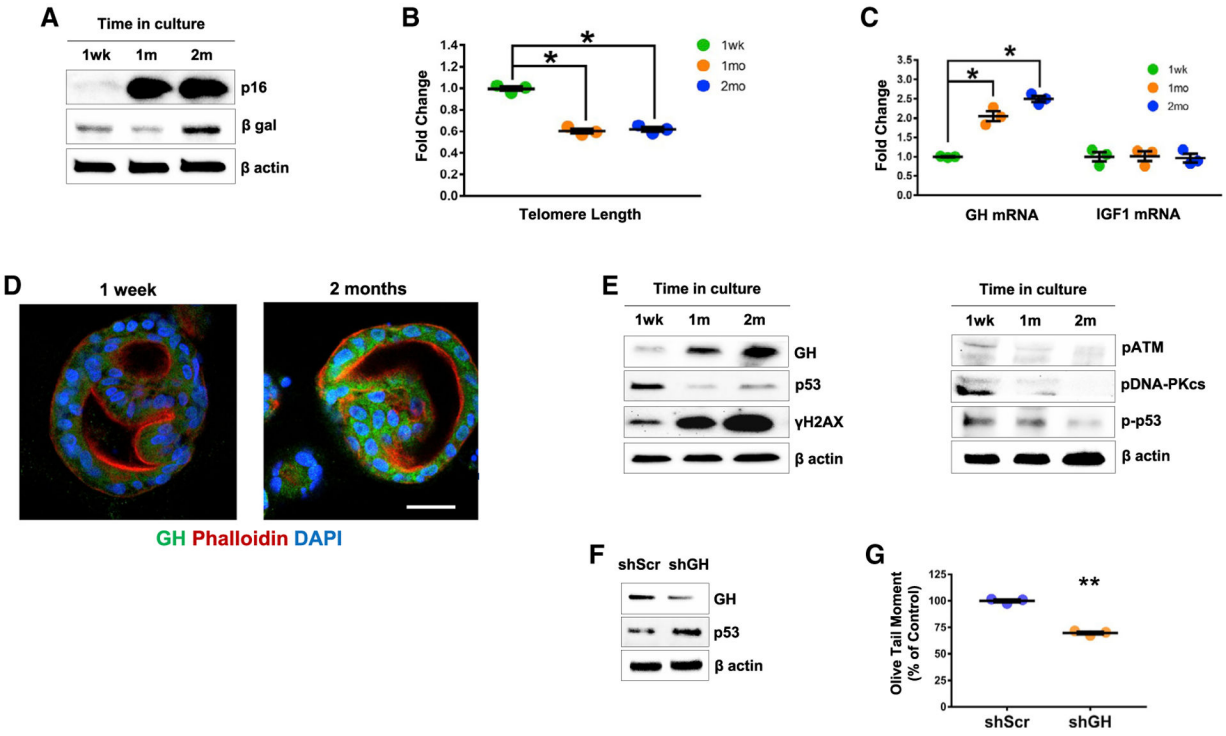

Figure 6. GH induction in aged organoids is associated with increased DNA damage

(A–C) Human intestinal organoids were cultured for up to 2 months and assessed on (A) western blot for aging markers p16 and β gal, and (B and C) real-time PCR for changes in (B) telomere length with culturing reflecting aging and (C) GH and IGF1 mRNA. PCR results are expressed as fold change versus control taken as 1. Results are shown as means ± SEMs of triplicate measurements. Each dot represents 1 experiment. In (B) and (C), results were analyzed by ANOVA, followed by Tukey's test to correct for multiple group comparisons. Results are graphed as fold change, but statistical testing was performed on raw numbers. *$p < 0.05$.

(D) Representative confocal image of organoids at 1 week and 2 months of culture. GH, green; phalloidin, red; DAPI, blue. Scale bar, 50 μm.

(E) Western blot analysis of GH, p53, and γH2AX and DNA damage pathway proteins. ImageJ quantification of western blots is depicted in Figure S5B.

(F and G) Organoids were cultured for 2 months, infected with lenti GH shRNA (shGH) or scramble (shScr), and analyzed 6 days later.

(F) Western blot of GH and p53 protein expression. ImageJ quantification of western blots is depicted in Figure S7.

(G) Comet assay. Each dot represents 1 independent experiment. Mixed model regression was used to adjust for random effects across experimental replicates. Results are graphed as percentage of control, but statistical testing was performed on raw numbers. **$p < 0.01$.

In (A), (D), and (E), representative blots from at least 3 independent experiments are shown.

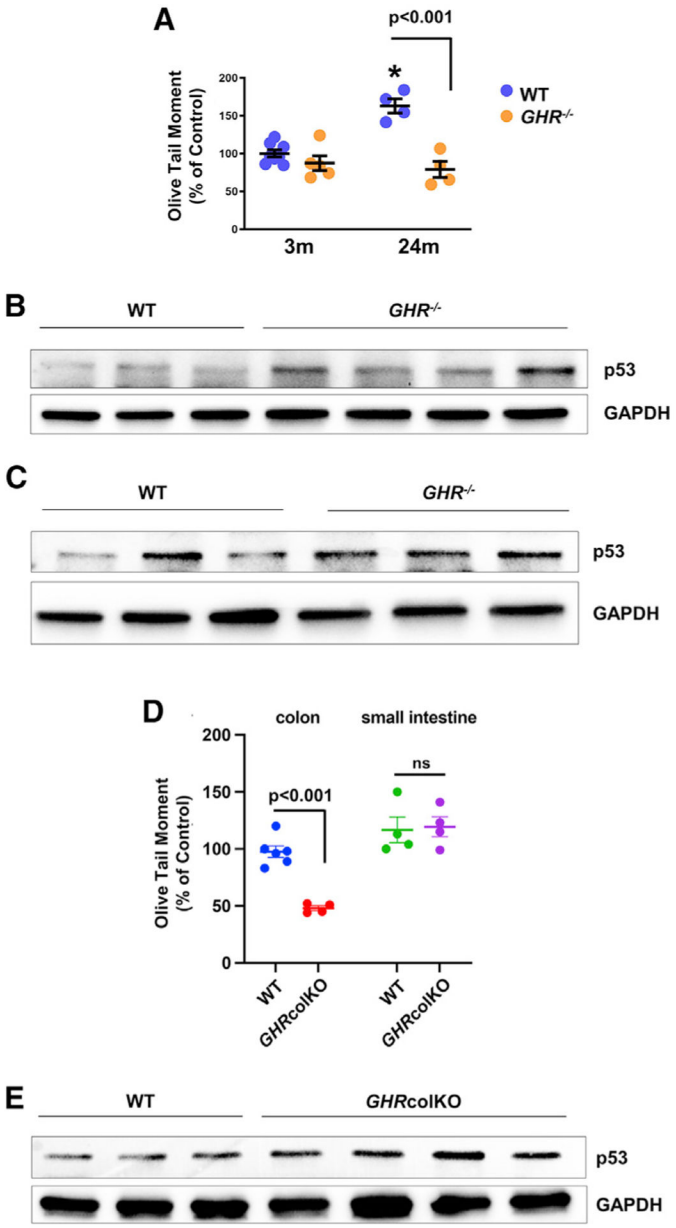

Figure 7. Abrogated GH signaling reduces DNA damage in aging mouse colon

(A) Comet assay in the colon of young (3 months) and old (24 months) WT and *GHR*$^{-/-}$ mice. *p < 0.0001 WT old versus both WT and *GHR*$^{-/-}$ young mice.

(B and C) Western blot of p53 in the colons of old (B) male and (C) female WT and *GHR*$^{-/-}$ mice.

(D) Comet assay in colons (with *GHR* excision) and in small intestines (with intact *GHR*) of 20-month-old *GHR*colKO and control (C) male mice. Results were analyzed by ANOVA followed by Tukey's multiple comparison test. Results are graphed as percentage of control, but statistical testing was performed on raw numbers.

(E) Western blot of p53 in the colon of WT and *GHR*colKO mice. ImageJ quantifications of western blots are depicted in Figure S7.

In (A) and (D), each dot represents 1 individual animal.

KEY RESOURCES TABLE

REAGENT or RESOURCE	SOURCE	IDENTIFIER
Antibodies		
Mouse anti-TRIM29/ATDC (H-300)	SCBT	Cat# sc-33151; RRID: AB_2209926
Rabbit anti-TRIM29/ATDC	Cell Signaling Technology	Cat# 5182; RRID: AB_10621949
Mouse anti-phospho-ATM (Ser1981) (clone 10H11.E12/05)	MilliporeSigma	Cat# 05-740; RRID: AB_309954
Rabbit anti-phospho-ATM (Ser1981)	Cell Signaling Technology	Cat# 13050; RRID: AB_2798100
Rabbit anti-phospho-histone H2A.X (Ser139)	Cell Signaling Technology	Cat# 9718; RRID: AB_10121789
Mouse anti-phospho-histone H2A.X (Ser139) (clone JBW301)	Millipore	Cat# 05-636; RRID: AB_309864
Mouse anti-phospho-p53 (Ser15) (clone 16G8)	Cell Signaling Technology	Cat# 9286; RRID: AB_331741
Mouse anti-Tip60 (C7)	SCBT	Cat# sc-166323; RRID: AB_2296327
Rabbit anti-GAPDH (14C10)	Cell Signaling Technology	Cat# 2118; RRID: AB_561053
Rabbit anti-phospho-DNA-PKcs (Thr2609)	SCBT	Cat# sc-101664; RRID: AB_2300400
Rabbit anti-phosho-STAT5 (Tyr694)	Cell Signaling Technology	Cat# 4322; RRID: AB_10548756
Mouse anti-p16 (F12)	SCBT	Cat# sc-1661; RRID: AB_628067
Mouse anti-beta-galactosidase (clone 10B2)	LS Bio	Cat# LS-B10989
Goat anti-growth hormone	R&D Systems	Cat# AF1067; RRID: AB_354573
Rabbit anti-growth hormone	LS Bio	Cat# LS-B4199; RRID: AB_10719011
Rabbit anti-rat growth hormone	A.F. Parlow National Hormone and Peptide Program	Cat# rat pituitary growth hormone; RRID: AB_2629219
Mouse anti-beta-actin (clone AC-15)	MilliporeSigma	Cat# A1978 RRID: AB_476692
Rabbit anti-p21	Cell Signaling Technology	Cat# 2947; RRID: AB_823586
Mouse anti-alpha-smooth muscle actin (clone 1A4)	Sigma-Aldrich	Cat# A2547; RRID: AB_476701
Goat anti-alpha-smooth muscle actin	Abcam	Cat# ab21027; RRID: AB_1951138
Goat anti-human GHR	R&D Systems	Cat# AF1210; RRID: AB_2294700
ECL anti-mouse IgG, HRP, made in sheep	Amersham	Cat# NA931
ECL anti-rabbit IgG, HRP, made in sheep	Amersham	Cat# NA934
Donkey anti-goat IgG, HRP	Jackson ImmunoResearch	Cat# 805-035-180
Alexa Fluor 568 donkey anti-rabbit IgG	Invitrogen	Cat# A-10042
Alexa Fluor 488 donkey anti-mouse IgG	Invitrogen	Cat# A-21202
Alexa Fluor 488 goat anti-rabbit IgG	Invitrogen	Cat# A-32731
Bacterial and virus strains		
pLV-EF1p-hGH1-IRES-eGFP-WPRE lentiviral particles	Regenerative Medicine Institute at Cedars-Sinai Medical Center	N/A
pLV-EF1p-mCherry-IRES-eGFP-WPRE lentiviral particles	Regenerative Medicine Institute at Cedars-Sinai Medical Center	N/A
mCMV-hGH1-RFP-HYGRO lentiviral particles	Regenerative Medicine Institute at Cedars-Sinai Medical Center	N/A
mCMV-RFP-HYGRO lentiviral particles	Regenerative Medicine Institute at Cedars-Sinai Medical Center	N/A
GH1 shRNA (human) lentiviral particles	SCBT	Cat# sc-43803-V
Control shRNA lentiviral particles - A	SCBT	Cat# sc-108080
Biological samples		

REAGENT or RESOURCE	SOURCE	IDENTIFIER
Paraffin-embedded slides of human adenocarcinoma specimens of patients before and after treatment	Cedars-Sinai Biobank and Translational Research Core	N/A
Paraffin-embedded slides of human non tumorous colon tissue	Cedars-Sinai Biobank and Translational Research Core	N/A
Paraffin-embedded slides of human non tumorous colon tissue	iSpecimen	N/A
Colon Tissue Array	US Biomax	Cat# BC05002
Colon Tissue Array	US Biomax	Cat# CO806
Colon Tissue Array	US Biomax	Cat# CO809
Chemicals, peptides, and recombinant proteins		
Nutlin-3	Sigma-Aldrich	Cat# N6287
Etoposide	Sigma-Aldrich	Cat# E1383
Activin A	R&D Systems	Cat# 338-AC
Wnt3A	R&D Systems	Cat# 5036-WN
CHIR 99021	Tocris	Cat# 4423/10
FGF4	R&D Systems	Cat# 2035-F4
Noggin	R&D Systems	Cat# 6057-NG
Matrigel	Corning	Cat# 354234
EGF	R and D Systems	Cat# 236-EG
A83301	Tocris	Cat# 2939
SB 202190	Tocris	Cat# 1264
TrypLE	ThermoFisher Scientific	Cat# 12604013
Y-27632	Sigma-Aldrich	Cat# Y0503
B27	GIBCO	Cat# 17504044
CD326 MicroBeads (EpCAM)	Miltenyi Biotec	Cat# 130-061-101
ROCK inhibitor	Tocris	Cat# 1254
Cell Recovery Solution	Corning	Cat# 354253
IntestiCult Organoid Growth Medium	STEMCELL Technologies	Cat# 06010
PriGrow III media	Applied Biological Materials	Cat# TM003
mTeSR1 media	Stem Cell Technology	Cat# 85850
Advanced DMEM12	GIBCO	Cat# 12634010
Complete Fibroblasts Growth Media	CellBiologics	Cat# M2267
Primocyn antibiotic solution	Invitrogen	Cat# ant-pm-2
ECL Cell Attachment Matrix	MilliporeSigma	Cat# 08-110
EdU	ThermoFisher	Cat# C10337
Polybrene	SCBT	Cat# sc-134220
AlexaFluor-647 phalloidin	Invitrogen	Cat# A22287
ProLong Gold antifade reagent with DAPI	Invitrogen	Cat# P36935
DAPI	Sigma-Aldrich	Cat# 10236276001
MTT	Sigma-Aldrich	Cat# M5655
Trizol	Invitrogen	Cat# 15596018
SsoAdvanced Universal SYBR Green SuperMix	Bio-Rad Laboratories	Cat# 1725274
Critical commercial assays		
Human GH ELISA kit	R&D Systems	Cat# DGH00

REAGENT or RESOURCE	SOURCE	IDENTIFIER
5-Bromo-2′-deoxy-uridine Labeling and Detection Kit I	Roche	Cat# 11296736001
Relative Telomere Length Quantification qPCR Assay Kit (human)	ScienCell Research Laboratories	Cat# 8908
Hikari Signal Enhancer Kit for primary and secondary antibody	Nacalai USA	Cat# NU00102
ImmPress Excel Staining Kit-Peroxidase	Vector	Cat# MP-7601
RNAeasy mini Kit	QIAGEN	Cat# 74104
SuperScript II First-Strand cDNA Synthesis System	ThermoFisher	Cat# 18091050
OxiSelect Comet Assay Kit	Cell Biolabs	Cat# STA-350
RNAscope VS Reagent Kit -RED	ACD Bio	Cat# 539089
Amaxa Basic Nucleofector Kit for Primary Mammalian Epithelial Cells	Lonza	Cat# VPI-1005
Senescence Cells Histochemical Staining Kit	Sigma-Aldrich	Cat# CS0030
Experimental models: organisms/strains		
Mouse: C57BL/6 J	The Jackson Laboratory	Stock ID#00064; IMSR_JAX:000664
Mouse: FVB/NJ	The Jackson Laboratory	Stock ID# 001800
Mouse: B6N[Cg]-Ghr < tm1b(KOMP)Wtsi > /3J	The Jackson Laboratory	Stock ID# 021486
Mouse: C57BL/6-Tg(car1-cre)	The Jackson Laboratory	Stock ID# 016097
Mouse: GHR flox/flox (Ghr < tm1b(KOMP) Wtsi >)	UC Davis KOMP Repository	Design ID: 49728
Oligonucleotides		
GH1 siRNA (human)	SCBT	Cat# sc-43803
Control siRNA	SCBT	Cat# sc-37007
Human GH forward CAGCAACGTCTATGACCTCC	Invitrogen	Cat# 10336022
Human GH reverse CTTGAAGATCTGCCCAGTCC	Invitrogen	Cat# 10336022
Human IGF1	QIAGEN	Cat# PPH00167C-200, lot# 201710060394
Human prolactin	Bio-Rad laboratories	Unique Assay ID: qHsaCID0015557
Human GAPDH	Bio-Rad laboratories	Unique Assay ID: qHsaCEP0041396
Human actin forward CTCCTTAATGTCACGCACGAT	Invitrogen	N/A
Human actin reverse CATGTACGTTGCTATCCAGGC	Invitrogen	N/A
Human GH1 mRNA probe for RNAscope	ACD Bio	Cat# 539081
Recombinant DNA		
Human Growth Hormone	Genewiz	This paper
pcDNA 3.1 vector	Invitrogen	Cat# V79020
pIRES2-ZsGreen1 vector	Clontech	Cat# NC1864918
pZip-mCMV-RFP-Puro	Transomic	N/A
pCBASceI	Addgene	Cat# 26477; RRID: Addgene_26477
NHEJ reporter cassette	Dr. Vera Gorbunova	vgorbuno@UR.Rochester.edu
HR reporter cassette	Dr. Vera Gorbunova	vgorbuno@UR.Rochester.edu
pDsRed2-N1	Clontech	Cat# 632406
Software and algorithms		
GraphPad Prism 7	GraphPad Software	https://www.graphpad.com/scientific-software/prism/
Fiji ImageJ V2.0	Open source	https://imagej.net/software/fiji/

REAGENT or RESOURCE	SOURCE	IDENTIFIER
CFX Maestro 1.0	Bio-Rad Laboratories	Cat# 12004110
FlowJo	TreeStar	https://www.flowjo.com/
Image Lab	Bio-Rad Laboratories	Cat# 17006130
Other		
Colon Intestine-Chips	Emulate Inc.	Cat# 10231-2
Lab-Tek Chamber Slide System	ThermoFisher Scientific	Cat# 154534, lot# 092013 80
Amaxa Nucleofector I	Lonza	Cat# AAD-1001S
Trans-Blot Turbo Transfer System	Bio-Rad Laboratories	Cat# 1704150
Molecular Imager ChemiDoc XRS Plus Imaging System	Bio-Rad Laboratories	Cat# 1708265
CFX96 Touch Real Time PCR System	Bio-Rad Laboratories	Cat# 1845096
S1000 Thermal Cycler	Bio-Rad Laboratories	Cat# 1852148
FACSAria cell sorter	BD Biosciences	N/A
FACS-Canto	BD Biosciences	N/A
OPTICA IM-3LD2 Trinocular Inverted LED Epi-Fluorescence Microscope	Leica Microsystems	Cat# OPIM-3LD2
Stellaris Confocal Microscope	Leica Microsystems	https://www.leica-microsystems.com/ppc/confocal
Inverted laser scanning confocal microscope Zeiss LSM 880 (objective: Zeiss LD Plaa- Neofluar 20X/0.40 Korr M27)	Zeiss	https://www.micro-shop.zeiss.com/en/us/shop/objectives/421351-9972-000/Objective-LD-Plan-Neofluar-20x-0.4-Corr-Ph2-M27